PAPER • OPEN ACCESS

JET D-T scenario with optimized non-thermal fusion

To cite this article: M. Maslov *et al* 2023 *Nucl. Fusion* **63** 112002

OPEN ACCESS
IOP Publishing | International Atomic Energy Agency Nuclear Fusion
Nucl. Fusion **63** (2023) 112002 (22pp) https://doi.org/10.1088/1741-4326/ace2d8

JET D-T scenario with optimized non-thermal fusion

M. Maslov[1,*], E. Lerche[1,2], F. Auriemma[3,16], E. Belli[4], C. Bourdelle[5], C.D. Challis[1], A. Chomiczewska[6], A. Dal Molin[7], J. Eriksson[8], J. Garcia[5], J. Hobirk[9], I. Ivanova-Stanik[6], Ph. Jacquet[1], A. Kappatou[9], Y. Kazakov[2], D.L. Keeling[1], D.B. King[1], V. Kiptily[1], K. Kirov[1], D. Kos[1], R. Lorenzini[3], E. De La Luna[10], C.F. Maggi[1], J. Mailloux[1], P. Mantica[7], M. Marin[11], G. Matthews[1], I. Monakhov[1], M. Nocente[7,12], G. Pucella[13], D. Rigamonti[7], F. Rimini[1], S. Saarelma[1], M. Salewski[14], E.R. Solano[10], Ž. Štancar[1], G. Stankunas[15], H. Sun[1], M. Tardocchi[7], D. Van Eester[2] and JET Contributors[a]

[1] UKAEA, Culham Science Centre, Abingdon OX143DB, United Kingdom of Great Britain and Northern Ireland
[2] Laboratory for Plasma Physics, ERM/KMS, B-1000 Brussels, Belgium
[3] Consorzio RFX (CNR, ENEA, INFN, Università di Padova, Acciaierie Venete SpA), Corso Stati Uniti 4, Padova 35127, Italy
[4] General Atomics, PO Box 85608, San Diego, CA 92186-5608, United States of America
[5] CEA, IRFM, F-13108 St-Paul-Lez-Durance, France
[6] Institute of Plasma Physics and Laser Microfusion, Hery 23, 01-497 Warsaw, Poland
[7] Institute for Plasma Science and Technology, CNR, via Cozzi 53, 20125 Milan, Italy
[8] Department of Physics and Astronomy, Uppsala University, SE-75120 Uppsala, Sweden
[9] Max-Planck-Institut für Plasmaphysik, Boltzmannstr. 2, 85748 Garching, Germany
[10] Laboratorio Nacional de Fusión, CIEMAT, 28040 Madrid, Spain
[11] EPFL, Swiss Plasma Center (SPC), CH—1015 Lausanne, Switzerland
[12] Department of Physics, University of Milano-Bicocca, Piazza della Scienza 3, 20126 Milan, Italy
[13] ENEA C. R. Frascati, via E. Fermi 45, 00044 Frascati (Roma), Italy
[14] Department of Physics, Technical University of Denmark, Kgs. Lyngby, Denmark
[15] Lithuanian Energy Institute, Laboratory of Nuclear Installation Safety, Kaunas, Lithuania
[16] Istituto per la Scienza e la Tecnologia dei Plasmi del CNR, Corso Stati Uniti 4, Padova 35127, Italy

E-mail: mikhail.maslov@ukaea.uk

Received 24 April 2023, revised 12 June 2023
Accepted for publication 29 June 2023
Published 12 October 2023

Abstract

In JET deuterium-tritium (D-T) plasmas, the fusion power is produced through thermonuclear reactions and reactions between thermal ions and fast particles generated by neutral beam injection (NBI) heating or accelerated by electromagnetic wave heating in the ion cyclotron range of frequencies (ICRFs). To complement the experiments with 50/50 D/T mixtures maximizing thermonuclear reactivity, a scenario with dominant non-thermal reactivity has been developed and successfully demonstrated during the second JET deuterium-tritium campaign DTE2, as it was predicted to generate the highest fusion power in JET with a Be/W wall. It was

[a] See the author list of "Overview of T and D-T results in JET with ITER-like wall" by C.F. Maggi *et al* to be published in *Nuclear Fusion Special Issue: Overview and Summary Papers from the 29th Fusion Energy Conference (London, UK, 16–21 October 2023).*
[*] Author to whom any correspondence should be addressed.

performed in a 15/85 D/T mixture with pure D-NBI heating combined with ICRF heating at the fundamental deuterium resonance. In steady plasma conditions, a record 59 MJ of fusion energy has been achieved in a single pulse, of which 50.5 MJ were produced in a 5 s time window ($P_{\rm fus} = 10.1$ MW) with average $Q = 0.33$, confirming predictive modelling in preparation of the experiment. The highest fusion power in these experiments, $P_{\rm fus} = 12.5$ MW with average $Q = 0.38$, was achieved over a shorter 2 s time window, with the period of sustainment limited by high-Z impurity accumulation. This scenario provides unique data for the validation of physics-based models used to predict D-T fusion power.

Keywords: tokamak, nuclear fusion, tritium

(Some figures may appear in colour only in the online journal)

1. Introduction

The second major deuterium-tritium (D-T) experimental campaign (DTE2) has been conducted at JET with Be/W wall (JET-ILW) in 2021. One of the main goals was to demonstrate a steady ELMy H-mode plasma with high fusion yield sustained over a 5 s duration. Two main scenarios, hybrid and baseline, were developed for that purpose [1, 2], both utilizing 50/50 deuterium/tritium (D/T) plasma mixtures as well as equally split neutral beam injection (NBI) heating power D-NBI and T-NBI. In this fuel mixture, the thermonuclear reactivity is maximised to the best possible extent reproducing the conditions in large future fusion reactors such as ITER or DEMO. Thermonuclear reactions are defined as interactions between D and T ions that are part of the Maxwellian bulk ion distribution. The fusion power generated in JET D-T plasmas always has a significant contribution from non-thermal fusion reactions—where one of the reactants is part of a supra-thermal ion population. In this work we define beam-target reactions as reactions between thermal ions and fast ions generated by the NBI heating. Similarly, radiofrequency (RF) tail—thermal reactions arise from the collisions between fast fuel ions accelerated by RF heating and the Maxwellian ion background.

The typical bulk ion temperatures achieved in the JET D-T plasmas ($T_{\rm i} \sim 10$ keV) are on the rising slope of the D-T fusion reaction cross-section. In these conditions, beam-target reactions have a strong contribution to the total fusion power produced since the neutral beam ions are injected at energies close to the optimum for D-T reactions (100–120 keV). Data on cross-sections of fusion reactions as a function of kinetic energy of an incident D on a stationary target can be found e.g. in [3]. The probability of these reactions is much larger than that of the thermonuclear reactions and even a relatively small number of fast NBI ions in the plasma can generate a comparable amount of fusion power. Ion cyclotron range of frequency (ICRF) heated ions are also typically accelerated to $E > 100$ keV but the number of particles in this energy range depends on the ICRF scenario and the density of the heated ion species. In the case of fundamental D heating of a large minority (10%–20%), the fusion enhancement due to RF acceleration of the D ions can be considerable.

In the highest performance JET-ILW plasmas with 50/50 D/T, the thermonuclear and beam-target contributions to the total fusion power are comparable. Hybrid scenarios have a lower plasma current, lower density and better penetration of NBI particles into the plasma core compared to the baseline H-modes which feature higher plasma current, higher density and weaker beam penetration. Hence hybrid scenarios tend to have a stronger beam-target contribution. In comparison, baseline scenarios tend to exhibit higher stored thermal energy for similar input power, so the thermonuclear component is higher whereas the beam-target component lower due to the less favourable deposition of NBI heating. The total fusion power anticipated in hybrid and baseline plasmas is nevertheless expected to be comparable, with a higher ratio of thermonuclear to beam-target reactions expected in baseline plasmas.

In order to access even higher fusion power and neutron production in JET plasmas, another approach has been adopted in addition to the 50/50 D/T scenarios: maximize the total fusion power by substantially increasing the beam-target reactions at the expense of thermonuclear reactions [4]. This was achieved by using pure D-NBI heating, fundamental D ion ICRF heating and altering the plasma isotope composition towards higher tritium concentration. The thermonuclear fusion power is given by

$$P_{\rm thermonuclear} = f_{\rm T}\,(1 - f_{\rm T})\, n_{\rm e}^2 < \sigma v >_{\rm therm} * E_{\rm DT}$$

and the beam-target fusion power for injection of a D-NBI into a D-T plasma mixture is

$$P_{\rm beam-target} = f_{\rm T}\, n_{\rm D-beam}\, n_{\rm e} < \sigma v >_{\rm beam} * E_{\rm DT}$$

where $f_{\rm T} = n_{\rm T}/(n_{\rm D} + n_{\rm T})$ is the tritium fraction, $n_{\rm e}$ the electron density, $<\sigma v>$ the reactivity and $E_{\rm DT}$ the fusion energy of the D-T reaction. The thermonuclear power is a parabolic function of $f_{\rm T}$ with a maximum at $f_{\rm T} = 0.5$, and the beam-target power is a linear function of $f_{\rm T}$ which reaches the maximum for a pure tritium plasma $f_{\rm T} = 1.0$. The total fusion power $P_{\rm fus} = P_{\rm therm} + P_{\rm beam\text{-}tar}$ reaches its highest value in the tritium-rich range of the D/T isotope ratio ($f_{\rm T} = 0.5$–1.0). The exact value of the optimal $f_{\rm T}$ as well as the magnitude of the fusion power increase with respect to the 50/50 D/T plasma depends on the relative contribution of the beam-target component. Plasmas with strong beam-target fusion component at 50/50 D/T will benefit most from shifting the isotope composition towards tritium-rich as the gain in beam-target fusion power will outweigh the loss in thermonuclear power.

Therefore, the hybrid scenario was utilized for this experiment in JET DTE2.

Hybrid and baseline 50/50 D/T scenarios used balanced D- and T-NBI heating which delivered similar amounts of T and D particles into the plasma. This approach ensured that the isotope composition in the hot plasma core does not deviate appreciably from the desired balanced 50/50 mixture. Heating a multiple ion component plasma with a single species NBI poses the additional challenge of controlling the isotope composition in the plasma core. At JET, NBI heating delivers significant particle fuelling: 2.5–3 $\times$ 10^{21} electrons/s at full power of $P_{\mathrm{NBI}} = 30$ MW. The JET D-T hybrid scenarios with plasma currents of 2.3 MA contains $\sim$3 $\times$ 10^{21} electrons, i.e. the time scale of replacing the ions in the plasma by ions from fuelling provided by NBI is of the order of 1 s. To maintain the low content of deuterium injected by NBI heating in a T-rich plasma over the target duration of 5 s, these ions must be efficiently removed from the plasma core after they have thermalized.

It has been shown previously at JET that the transport of ion components is much faster than the general plasma particle transport constrained by the electrons, when the transport is dominated by the ITG turbulence [5, 6]. In that case in a multi-ion plasma such as D/T mixture, the transport coefficients (diffusion D_{i} and convection V_{i}) of individual ion species are much larger than those of the electrons. Therefore, ions are much more readily moving across the magnetic flux surfaces, as long as the total ion density satisfies the ambipolarity constraint. This effect is also called fast ion mixing to emphasize the fact that the net ion particle flux across each magnetic surface $S_{\mathrm{inwards}} + S_{\mathrm{outwards}}$ is limited by the relatively slow transport of the electrons. One of the consequences of the fast ion mixing is the insensitivity of the isotope density profiles to the differences in the particle sources of the individual isotopes. As a part of preparation for this D-T experiment, it was demonstrated that the isotope transport is sufficiently strong even at the maximum NBI heating power to prevent the excessive accumulation of injected NBI species in the plasma core. Thus, a high tritium concentration could be maintained in the whole plasma volume and a high beam-target fusion reactivity could be achieved throughout the whole 5 s heating duration.

In addition to NBI, JET also has ICRF heating which was successfully used in all D-T scenarios, typically using fundamental harmonic heating of hydrogen or ^{3}He minorities [7, 8]. These heating schemes can impact the overall fusion reactivity in three ways: (i) via second harmonic acceleration of respectively D or T bulk ions (enhancement of fusion reactions between ion populations in the RF tail and thermal plasma); (ii) via interaction between the injected D- or T-NBI ions with thermal plasma (beam-target fusion enhancement); (iii) via collisional bulk ion heating (thermonuclear fusion enhancement). The moderate deuterium concentration in tritium-rich plasmas allows the use of a different heating scheme: namely heating at the fundamental ion-cyclotron resonance frequency of the deuterium ions, accelerating a fraction of the thermalized D ions to supra-thermal energies and accelerating the injected D-NBI ions via ICRF-NBI synergy [9]. That scheme has been demonstrated at JET previously during DTE1, in L-mode plasmas and in the absence of NBI heating. Strong ICRF driven fusion reactivity has been reported, with a Q-factor reaching $Q = 0.25$ at the optimal D/T ratio [10]. Implementation of this scheme in conjunction with the beam-target dominant fusion scenario in T-rich plasma has been successfully demonstrated as part of the experiment reported here and provided significant boost in the generated fusion power as compared to 50/50 D/T plasmas using mixed D-T NBI and standard ICRF heating schemes.

This paper is organized as follows: section 2 is dedicated to the experiments in H/D mixture plasma which were used as demonstration of isotope control prior to the D-T experiments, in section 3 the plasma scenario is described while section 4 shows the results of fundamental harmonic deuterium resonance scheme tests done in tritium-rich plasma at low power. Section 5 summarises the experimental results of the high fusion power D-T experiments. Section 6 is dedicated to the interpretative analysis of the experiments. Section 7 summarizes the predictive modelling which was done in support of this scenario and section 8 concludes the paper.

2. Plasma core isotope control in the presence of strong NBI fuelling

Prior to the T-rich scenario development, a proof of principle demonstration of plasma isotope control has been performed. It has previously been demonstrated in JET mixed isotope plasmas, with core NBI fuelling of one isotope and edge gas fuelling of the other, that the resulting isotope mix is not sensitive to the choice of isotope fuelled by core NBI, due to the so-called fast isotope mixing effect. However, the experimental evidence was based on H/D plasma mixtures at low plasma current in the range of $I_{\mathrm{p}} = 1.4$ MA and D-NBI heating at power levels of 8–12 MW.

In order to support the DTE2 scenario development, hydrogen plasma experiments heated with D-NBI have been performed at higher plasma current and higher heating power to demonstrate that fast isotope ion mixing still applies to the case of higher power and particle fluxes.

The experimental sequence started with a 2.4 MA, 2.8 T pure deuterium plasma ($n_{\mathrm{H}}/n_{\mathrm{e}} < 1\%$) heated with 24 MW of D-NBI. ICRF heating was not used in this experiment to avoid D-D neutron production from reactions between ions in the RF tail and the thermal ions which would complicate the data analysis. The values of the plasma current and the toroidal magnetic field were constrained by the elevated power threshold of the L-H transition in hydrogen plasmas. To maintain stationary ELMy H-mode free from heavy impurity accumulation [11], additional gas dosing releasing 5 $\times$ 10^{22} electron s^{-1} was injected from a gas injection module located in the divertor area. The first half of this discharge served as a pure deuterium reference for comparison with the subsequent pulses. During the flattop of the H-mode phase at $t = 10$ s (see figure 1), deuterium gas fuelling was replaced by hydrogen fuelling at the same gas flow rate. The isotope content as measured by $\mathrm{H}_\alpha/\mathrm{D}_\alpha$ line emission at the plasma edge began to change towards the higher hydrogen content and reached $n_{\mathrm{H}}/n_{\mathrm{e}} \sim 75\%$ after 1.5 s. The neutron rate generated by D-D reactions predominantly in

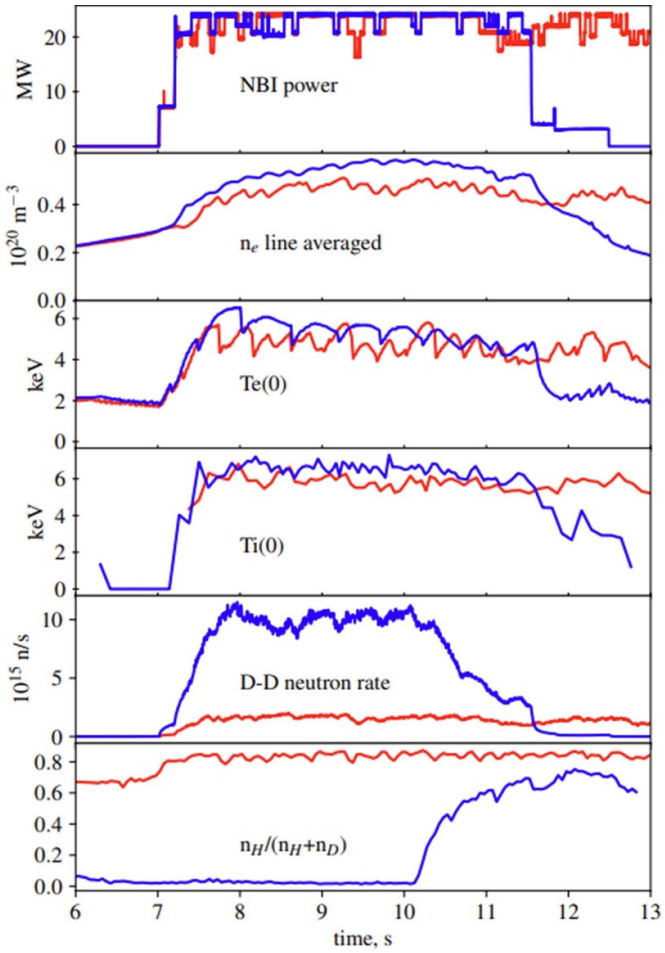

Figure 1. Demonstration of core isotope control in H-rich plasma with high power D-NBI heating. Blue: #94925, a 2.8 T, 2.4 MA pure D plasma with D-NBI heating with gas fuelling switching to pure hydrogen at 10 s, Red: #94926, a 2.8 T, 2.4 MA hydrogen-rich plasma with pure hydrogen gas fuelling and D-NBI heating, 85/15 H/D ratio as measured at the plasma periphery. A factor of 6 difference in D-D neutron rate indicates the lack of core D accumulation despite strong D-NBI fuelling.

the plasma core has responded promptly to the change of isotope content at the plasma boundary and decreased by a factor of 4 in the same time interval. The plasma stored energy as well as the core electron and ion temperatures only modestly responded to the change in isotope composition. Therefore, the observed D-D neutron rate decrease could only be attributed to the dilution of core plasma with the hydrogen injected as a gas.

Subsequent plasma pulses were done at the same plasma current and magnetic field but only hydrogen gas was injected during the H-mode phase and in the initial Ohmic phase. The only source of deuterium was the D-NBI heating. A stationary hydrogen-rich H-mode plasma with $n_H/n_e \sim 85\%$ was achieved, with the neutron rate at around 1/6th of the pure Deuterium reference pulse (see figure 1).

The core H/D composition of this plasma was inferred by matching the measured neutron rate to TRANSP [12–14] predictions, similar to the calculations described in [5]. Results are shown in figure 2. The best match to the observed neutron rate in the H-rich pulse was achieved in a TRANSP simulation with a low concentration of deuterium in the plasma core, $n_D/n_e \sim 20\%$ which is only slightly larger than the value measured at the plasma boundary by visible spectroscopy. Thus, the previously observed fast isotope ion mixing was confirmed for high power discharges: fast mixing of ion components is sufficiently strong to prevent core deuterium accumulation even in the plasmas relevant to high power D-T fusion production. This result was also supported by predictive integrated modelling, see section 7.

An important observation from this experiment is the change of plasma mixture from deuterium to hydrogen majority. Due to the low fuel retention of the metal wall in JET-ILW [15] and the high particle throughput of H-mode plasmas, a single plasma pulse was sufficient to switch from a pure deuterium to a hydrogen-rich plasma composition. This was also the case in D-T plasmas, where a fast switch from D-T to tritium-rich plasma composition was achieved, allowing the deuterium species to be maintained in the lower range of concentrations required to achieve high fusion power gain, as it will be shown in the following sections of this paper.

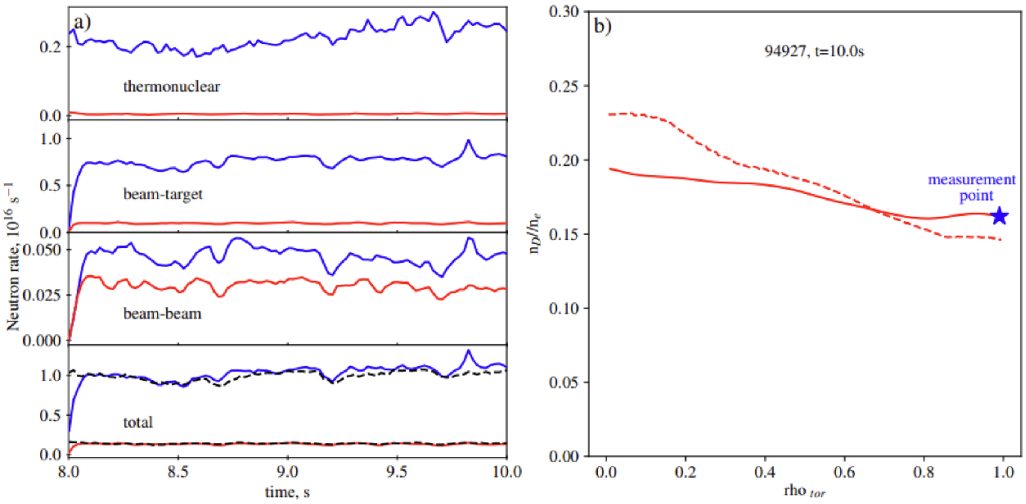

Figure 2. (*a*) Total neutron rate and its components (thermonuclear, beam-target and beam-beam) as calculated by a TRANSP simulation and comparison with the measured neutron rate (dashed). The simulations are done for pure deuterium plasmas (94925, blue) and hydrogen-rich plasmas (94927, red) (*b*) deuterium concentration profile of the hydrogen-rich plasma discharge, solid line—the input to the TRANSP simulation with neutron rate matching the experimental value, dashed line—results of predictive JINTRAC-QuaLiKiz simulation (see section 7).

3. D-T plasma scenario for high beam-target fusion power

3.1. Plasma D/T isotope composition

JET is equipped with 2 identical NBI beamlines which could be fed independently with either deuterium or tritium during the D-T campaign in 2021. Balanced (one injector fed with deuterium and the other one with tritium) NBI heating was used in the majority of DTE2 experiments, but both beamlines were supplied with deuterium for the experiment described in this work.

To support the basic estimates for the potential fusion power gain in the tritium-rich scenarios discussed in the introduction section, the TRANSP code [16] was used to calculate the beam-target versus thermonuclear fusion power for different plasma compositions and both options for the NBI configuration. For that assessment, a pure deuterium hybrid scenario pulse #86614 (2.9 T, 2.5 MA) was used [17]. TRANSP simulations were run in the interpretative mode, but all the kinetic profiles were modified with respect to those measured in #86614 with the aim to extrapolate to the maximum NBI power 32 MW available at JET with ILW. The methodology of the extrapolation is described in [17]. In the series of simulations described here, only the fuel mixture and NBI species were varied, with the density and temperature profiles kept the same. Thus, the effect of the isotope mass on the confinement was not accounted for in this scoping study.

The results are shown in figure 3. The thermonuclear reactivity peaks at a 50/50 plasma composition, as expected, and does not depend on the choice of the NBI species. In the case of mixed D + T NBI heating, the beam-target reactivity increases slightly towards a higher tritium content. At a beam energy of 100–120 keV for both species, the injection velocity is higher for deuterium, so that the reactivity is higher for fast deuterium as compared to fast tritium at the same energy. The optimal composition for the combined thermonuclear and beam-target reactivity is therefore slightly shifted from 50/50 D/T towards higher tritium concentration, but no significant variation of the fusion power occurs in a broad range of D/T ratios.

For the pure D-NBI case, the behaviour is very different. For a 50/50 D/T plasma, the fusion power is only slightly higher than for the mixed DT-NBI case due to more favourable beam-target reactivity with fast deuterium ions. The beam-target fusion power, on the other hand, strongly increases towards tritium rich plasma conditions so that the gain in power from beam-target reactions significantly outweighs the loss in thermonuclear power. The total fusion power is found to increase monotonically as the tritium concentration increases, reaching the maximum for the pure tritium case. According to this simulation, a nearly 50% gain in the total fusion power could be achieved in a hybrid scenario with respect to the 50/50 D/T case with D + T NBI species.

Analysis of the D-T fusion performance for various D/T plasma compositions and NBI species was also performed with the ETS heating and current drive (H&CD) workflow [18, 19], both for the baseline scenario [20] and for the hybrid-like plasmas described here [21]. The results are in qualitative agreement with those of figure 3 except that the maximum fusion reactivity with D-NBI only is not at $n_D/n_e = 0$ but peaks around $n_D/n_e = 10\%–20\%$ due to different assumptions on the plasma kinetic profiles.

Based on these predictions, scenarios with pure tritium gas fuelling and D-NBI were expected to provide the highest fusion power as they will achieve the maximum attainable tritium concentration with deuterium dilution coming solely from NBI injection and residual deuterium from previous plasma discharges.

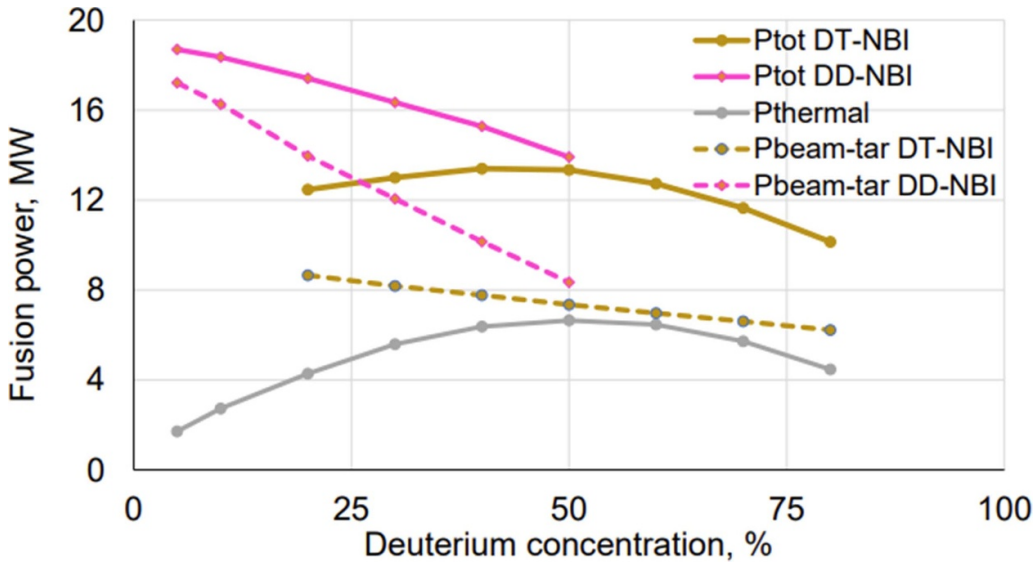

Figure 3. Thermonuclear and beam-target components of the total fusion power for different plasma isotope compositions and NBI configurations (gold: balanced DT NBI, magenta: pure D NBI).

3.2. Choice of toroidal magnetic field

Fundamental ICRF heating of deuterium requires half the RF frequency than the standard hydrogen minority scheme, so the range of frequencies available for this experiment was effectively limited to 28.5 MHz—the minimum available frequency where sufficiently high power can still be coupled to JET plasmas. At this frequency, the central deuterium cyclotron resonance requires the highest toroidal magnetic field accessible at JET. The exact choice of B_t was additionally constrained by the parasitic 2nd harmonic tritium resonance which must not be located in the proximity of the outer wall and the ICRF antennas (see figure 4). $B_t = 3.86$ T on-axis remained the best available option, as the 2nd harmonic tritium resonance would be found in a forbidden area for lower magnetic fields, and the required 6 s duration flat-top could not be sustained due to overheating of the toroidal field coils for higher magnetic fields.

Based on the above considerations, for the purpose of this experiment, a hybrid scenario [1] was adapted for higher values of the toroidal field (3.86 T instead of 3.4 T). The time evolution of B_t throughout the initial current ramp-up phase of the discharge had to be modified in order to minimise the heating of the toroidal field coils (see figure 5(*a*)). Both B_t waveforms were first used in test Ohmic pulses with the same plasma current waveform and the same plasma density. It was found that the target safety factor on-axis, $q(0)$, at the start time of the plasma current flattop ($t = 7.0$ s) in both cases are nearly identical. This could be identified by observation of the core sawtooth activity which starts when the $q = 1$ surface appears in the plasma following the relaxation of the current profile. In these two cases, the $q = 1$ surface appeared at the same time within 20 ms (figure 5(*b*)), even though a larger on-axis plasma current density was required at higher B_t to achieve the same value of $q(0)$. Therefore, no other changes to the hybrid scenario recipe for pre-tailoring of the current density profile were required.

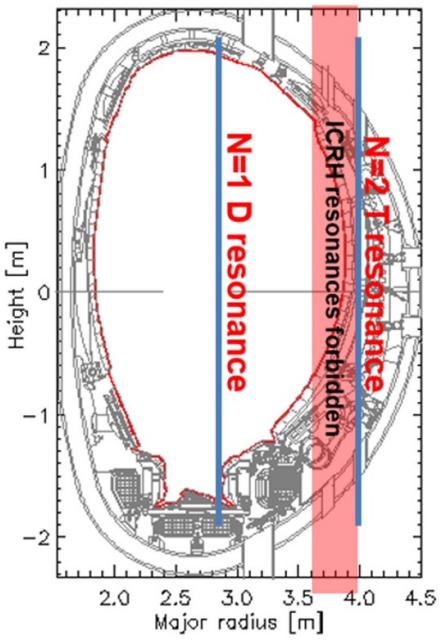

Figure 4. Position of ICRF resonances at JET for RF frequency $f = 28.5$ MHz and $B_t = 3.86$ T.

3.3. Comparison between hybrid scenarios at low and high B_t in pure tritium H-modes

As discussed in section 1, higher plasma current (3.0–3.5 MA in the baseline scenario) tends to produce a plasma scenario with increased thermonuclear part of the generated fusion

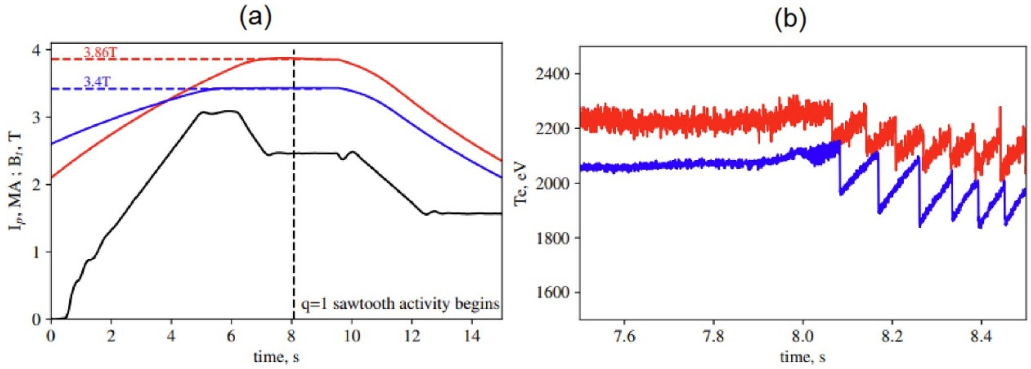

Figure 5. The effect of toroidal field ramp up on the target q-profile in cases of 3.4 T and 3.86 T. (*a*) B_t (red: #97587, blue #97586) and I_p (black, the same for both discharges) waveforms, (*b*) core electron temperature measured with the radiometer ECE, indicating the almost identical (within 20 ms) start time of sawtooth activity.

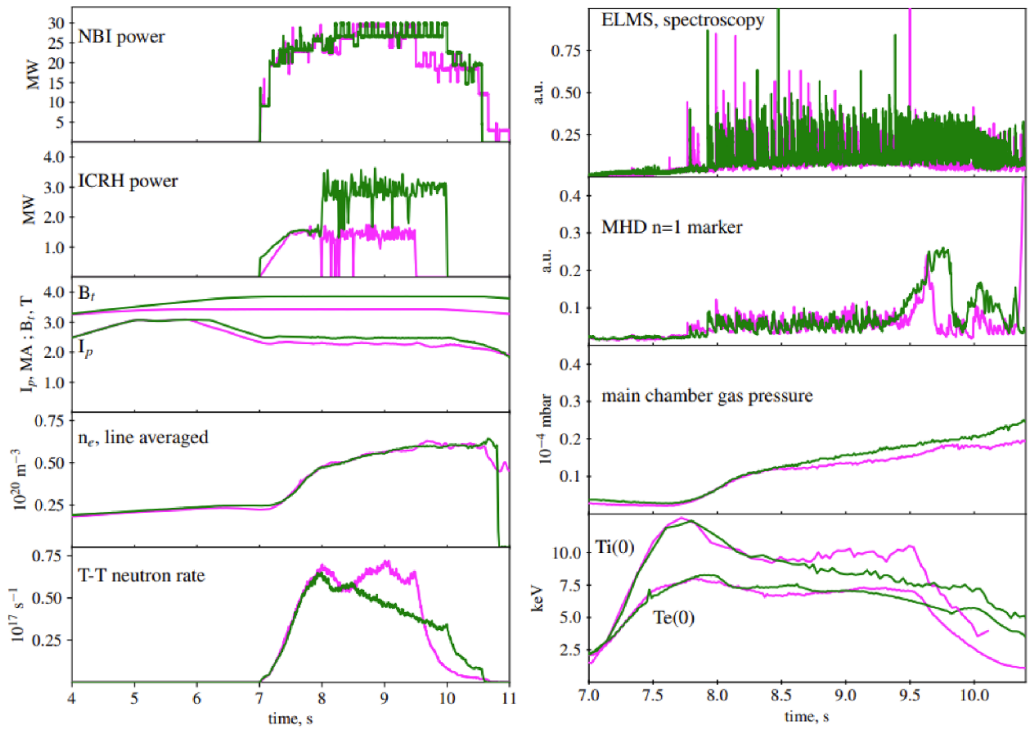

Figure 6. Reference pulses completed in pure tritium plasmas with T-NBI and hydrogen minority ICRF scheme, magenta: #99163, 2.3 MA, 3.4 T, green: #99172, 2.5 MA, 3.86 T.

power but decreased beam-target component, and therefore is not optimal for the tritium-rich plasma scenario. On the other hand, to maintain the tritium-rich isotope composition of the plasma over 5 s, a sufficient amount of tritium gas must be injected, of the order of 10 times more than the amount of deuterium injected by the NBI ($\sim 3 \times 10^{21}$ electrons s^{-1}). In type I ELMy H-mode plasmas the amount of gas fuelling required to maintain stationary conditions without compromising the energy confinement increases sharply with the plasma current [11]. Therefore, higher plasma current can be beneficial for the T-rich scenario as it allows achievement of higher tritium concentrations. As a compromise, the value of 2.5 MA was chosen for this experiment, as the extrapolations described in section 3.1 have shown that the enhancement of fusion power is still strong for this plasma current. The plasma current is larger here than in the 50/50 D/T hybrid scenario ($I_p = 2.3$ MA) but the value of q_{95} remained similar due to the proportionally larger toroidal magnetic field.

Prior to the DTE2 campaign, both scenarios (3.4 T, 2.3 MA and 3.86 T, 2.5 MA) were tested in pure tritium plasmas with T-NBI heating and a hydrogen minority ICRF heating scheme (at 51 MHz and 54.5 MHz frequencies for lower and higher B_t values, respectively). Results are shown in figure 6. Both pulses show similar behaviour and performance, except that the ion temperature and neutron production decreased in the pulse with higher B_t after the initial low gas/hot ion phase. This was caused by a slow increase of tritium gas pressure in

the vessel due to a different choice of the tritium gas injection. A continuous $n = 1$ mode appeared at $t = 9.4$–9.5 s in both discharges, once again indicating that the q profile shape and evolution were similar.

For the subsequent high fusion power D-T pulses, the tritium-rich scenario required only minor modifications from the pure T reference #99172 (shown in figure 6). The breakdown and Ohmic phases from 0 to 7 s remained the same, T-NBI heating was replaced by D-NBI, and the ICRF frequency was changed to 28.5 MHz to place the fundamental cyclotron resonance of D close to the magnetic axis. The heating phase was extended until 13 s with the expectation for the fusion power to reach the peak values at 8 s (see figure 6(*a*)) and to last for 5 s. A decrease in the requested gas dosing waveform was implemented throughout the H-mode phase to avoid the performance decrease observed in pulse #99172.

These adjustments did not require additional plasma pulses for implementation and testing, since re-development of the current ramp up phase and change in the timing of the gas dosing at the transition to the H-mode were not required (see [1] for the development of 50/50 D/T hybrid scenario). The only D-T plasma pulses performed for the purpose of these experiments prior to the high fusion power phase were focused on testing the ICRF heating scheme in L-mode plasmas, described in the next section. It allowed saving valuable operational time and saving 14 MeV neutron production within the overall 14 MeV neutron budget available for DTE2, which was a notable advantage of the tritium-rich scenario.

4. Demonstration of ICRF heating at the fundamental D cyclotron resonance frequency

As the ICRF heating scenario at the deuterium cyclotron frequency was selected for the tritium-rich experiments, proof-of-principle discharges were performed in L-mode plasmas to assess the heating efficiency and to improve the performance of the RF system hardware (generator tuning, impedance matching) at the operational RF frequency of 28.5 MHz prior to the high fusion power pulses. The relevant time traces of such a discharge are shown in the left column of figure 7. The right column shows the core ion temperature and fusion power for three different phases of the discharge: NBI only, ICRF only and combined NBI + ICRF. The toroidal magnetic field and the plasma current ($B_t = 3.86$ T, $I_P = 2.5$ MA) were the same as later used in the high-power H-mode discharges. A small amount of D_2 gas was injected to approach the isotope mixture expected in the presence of high power NBI ($n_D/n_e \sim 10\%$ from edge spectroscopy in this case).

The time traces in figure 7 show that the plasma stored energy (*b*) and the core ion temperature (*c*) respond to the NBI and ICRF power waveforms on a slower time scale than the fusion power (*d*), indicating that a large fraction of the neutrons comes from fast deuterium ions colliding with the thermal tritons, either when injected with NBI (∼100 keV) or when accelerated by ICRF. The ICRF heating efficiency values ($P_{abs}/P_{coupled}$) estimated from the break-in-slope analysis of the plasma energy response to steps in the ICRF power waveform [22] are given in figure 7(*b*) and confirm that the ICRF heating scenario at the fundamental deuterium cyclotron frequency is very efficient in these conditions. The heating efficiency values obtained slightly exceed 100% because of two effects: (i) the non-thermal contribution to the plasma stored energy signal is increased non-linearly by NBI + ICRH synergy during the RF switch-on and (ii) the alpha particle heating is also modified with the application of ICRH. Finally, the uncertainty of the break-in-slope analysis is around 10%. In fact, RF wave modelling shows that the single-pass absorption of the launched waves is already high in L-mode and is actually improved in H-mode (with larger plasma density and temperature) and in the presence of high NBI power. In such conditions, the fundamental D heating scheme is expected to work well at larger D concentrations [23].

The ion temperature response to the auxiliary power input (e) is similar for both heating methods (∼0.5 keV MW^{-1}) and the values achieved with combined NBI + ICRH heating follow a similar trend, showing that synergistic effects have a small impact on the plasma heating properties. The fusion power increase (*f*), on the other hand, is stronger with ICRF ($P_{fus}/P_{ICRH} = 0.2$) than with NBI only heating ($P_{fus}/P_{NBI} = 0.12$), indicating that a larger fraction of the bulk D ions is accelerated to D-T fusion relevant energies with 2.5 MW ICRF than when injected at $E = 100$ keV with 1.7 MW NBI (source rate $= 1.5 \times 10^{17}$ s^{-1}). More importantly, the fusion power values achieved with the combined NBI + ICRF heating are significantly higher than what one would expect by considering the average fusion enhancement due to ICRH or NBI alone ($P_{fus}/P_{NBI+CRH} = 0.27$), showing that the NBI + ICRF synergistic effects are playing an important role in the D-T neutron production in this pulse. The synergistic effect estimated from these data is ∼35% (see arrow in figure 7(*f*)) which was confirmed by theoretical modelling using NBI only, ICRF only and combined ICRF + NBI heating (see section 6 for ETS modelling).

5. The high fusion power T-rich experiments in JET DTE2

In total, nine high power T-rich hybrid H-mode pulses were performed in the JET-ILW DTE2 campaign, with different rates of gas fuelling and performance of NBI heating. The list of pulses is outlined in table 1. In pulse #99965, the ICRF power has been deliberately modulated to demonstrate the effect of the RF heating on the scenario performance. The combined fusion energy generated in this series of T-rich H-modes was 454.6 MJ, corresponding to 1.616×10^{20} 14 MeV neutrons, which constituted 19% of the total D-T neutrons generated in the DTE2 campaign. Pulse #99971 achieved the highest value of the total $E_{fus} = 59$ MJ, of which 50.5 MJ were generated within a 5 s time window giving the average $P_{fus} = 10.1$ MW. The 5 s averaged fusion production efficiency $Q = <P_{fus}>/<P_{in}>$ was 0.33 in this pulse. Here $<P_{in}>$ is the total heating power injected into plasma

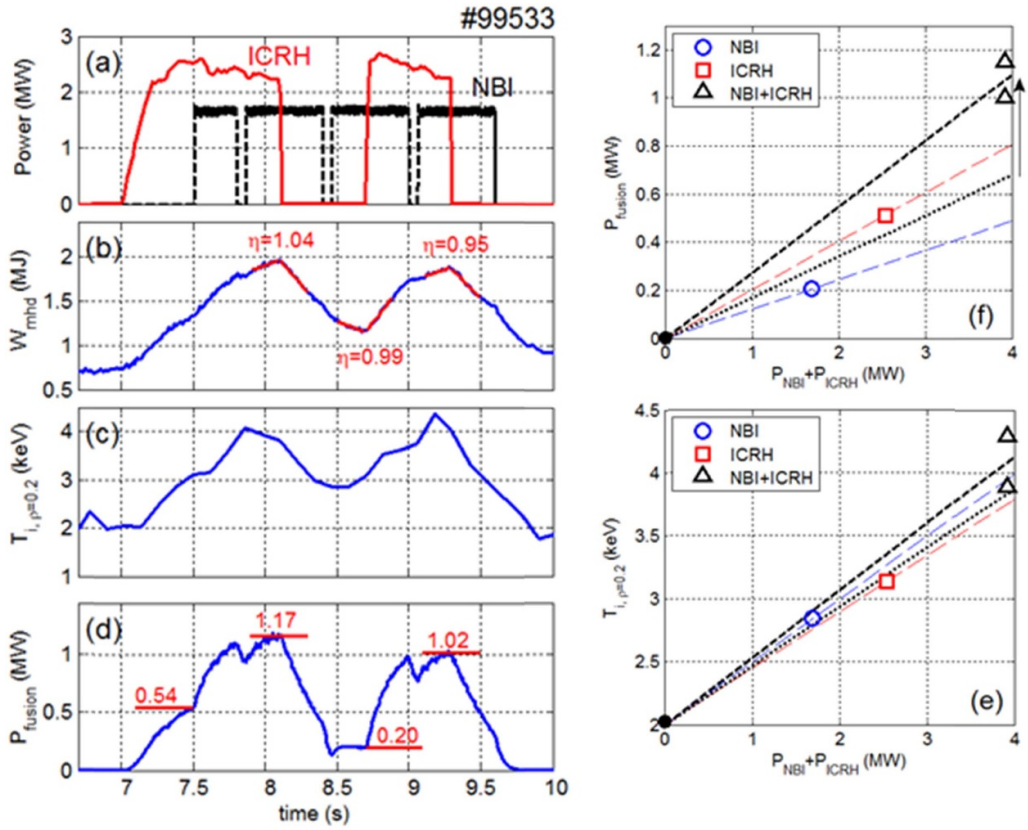

Figure 7. Time traces of main parameters in a T-rich L-mode discharge #99533 used to prove the $n = 1$ D RF heating scheme: (*a*) ICRF and NBI power; (*b*) Plasma stored energy, with red highlighted line indicating where the break-in-slope analysis was performed; (*c*) Core ion temperature ($\rho = 0.2$, crystal spectrometer); (*d*) Total fusion power. The right column shows the average core ion temperature (*e*) and the average fusion power (*f*) obtained with NBI-only ($t = 8.6$ s), ICRF-only ($t = 7.5$ s) and combined NBI + ICRF heating ($t = 8.1$ s and 9.3 s).

Table 1. Summary of high fusion power T-rich pulses produced in JET DTE2.

Pulse number	Total E_{fus} produced, MJ	Comments
99960	35.88	Stationary pulse, low performance
99962	46.05	High Z core impurity accumulation
99963	49.44	High Z core impurity accumulation
99964	54.24	Stationary pulse
99965	43.51	ICRH modulated, High Z core impurity accumulation
99969	54.83	High Z core impurity accumulation
99970	57.09	Stationary pulse
99971	58.99	Stationary pulse
99972	56.10	High Z core impurity accumulation

$P_{\mathrm{in}} = P_{\mathrm{NBI}} + P_{\mathrm{ICRH}} + P_{\mathrm{Ohmic}}$. The highest peak fusion performance was demonstrated in #99972, with $P_{\mathrm{fus}} = 12.5$ MW over a 2 s duration, with $Q = 0.38$. Seven pulses from this experiment have exceeded the highest E_{fus} value of 45.8 MJ achieved in 50/50 D/T scenarios with mixed D-NBI and T-NBI heating. The fusion performance of some of the T-rich hybrid pulses is illustrated in figure 8.

All pulses had approximately a 6 s long phase with high heating power aiming at producing stable fusion power over 5 s. The maximum D-NBI power injected was ∼29 MW but it could not be systematically reproduced for the full duration in each of the attempted pulses due to technical difficulties to reliably operate the NBI system at the maximum capability in each single JET pulse. The beam energy varied between the individual injectors in the range of 96–115 keV, with the average of 108 keV in pulse #99971. The power distributed between the first, second and third NB energy fractions were as follows: 0.53, 0.33, 0.14 with small variations between individual injectors. ICRF power of 4 MW at the fundamental deuterium cyclotron frequency was applied to all discharges of this series.

For the plasma gas fuelling, pure tritium gas was used with average flow rate of 1.7×10^{22} atoms s^{-1} during the flattop H-mode phase. Only 8.4×10^{20} atoms of deuterium gas was

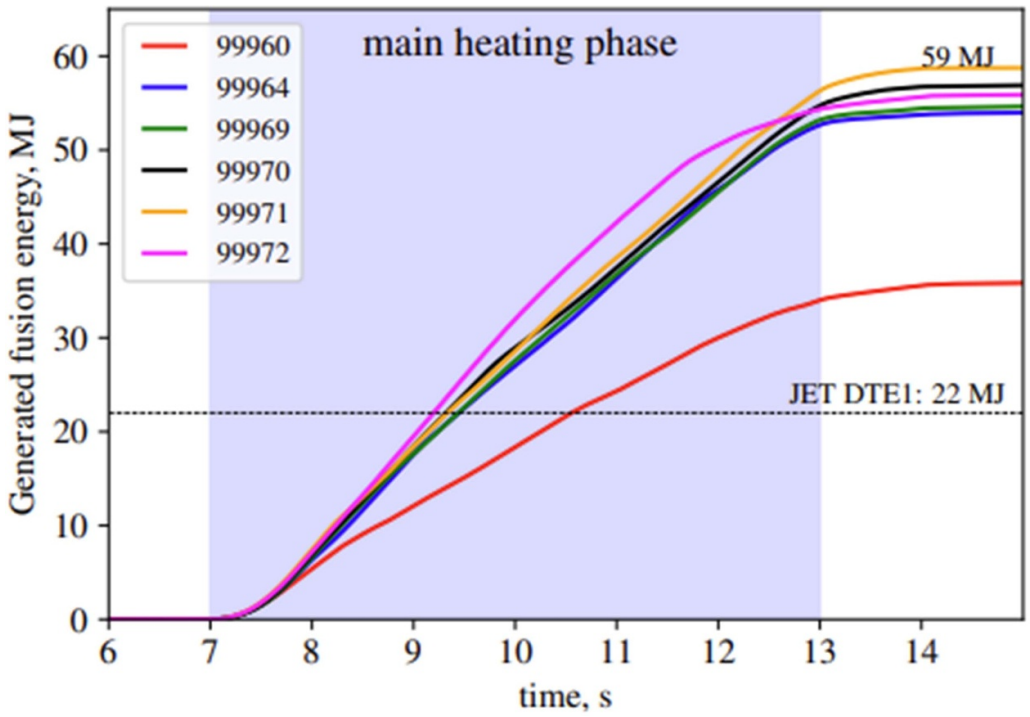

Figure 8. Summary of fusion energy generated in T-rich hybrid pulses. Five pulses generated substantially more than 50 MJ, with a record of 59 MJ. For comparison, the record fusion energy generated in a single pulse in the JET DTE1 campaign was 22 MJ [24].

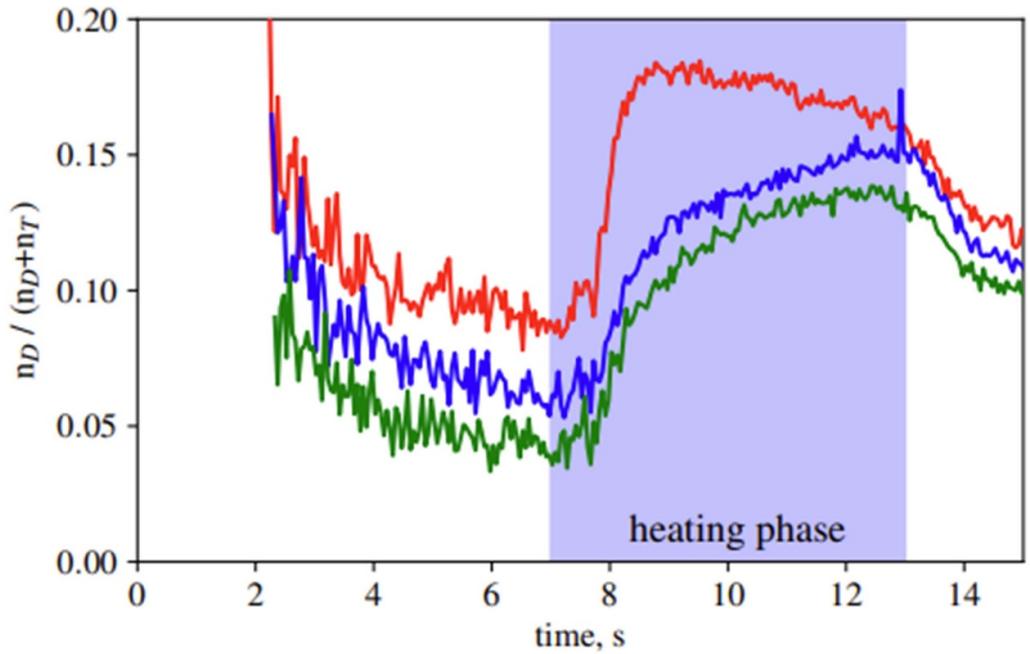

Figure 9. $n_D/(n_D + n_T)$ ratio as measured in subdivertor penning gauge spectroscopy in pulses #99960 (red), #99964 (blue) and #99972 (green).

injected as a pre-fill for the breakdown which had no significant effect on the D/T composition during the heating phase. The rest of deuterium has been injected by means of NBI heating at $\sim 2.7 \times 10^{21}$ atoms s^{-1} at maximum power.

The D/T isotope ratio, as measured by the subdivertor penning gauge discharge spectroscopy [25, 26], varied slightly between the pulses throughout the experiment, as shown in figure 9. The first pulse, #99960, had residual deuterium in the vessel walls and therefore the highest measured D/T ratio of about ~18/82 at the beginning of the heating phase, decreasing towards 15/85 at the end of the discharge. For the pulses later in the series, the wall content had shifted to a larger tritium

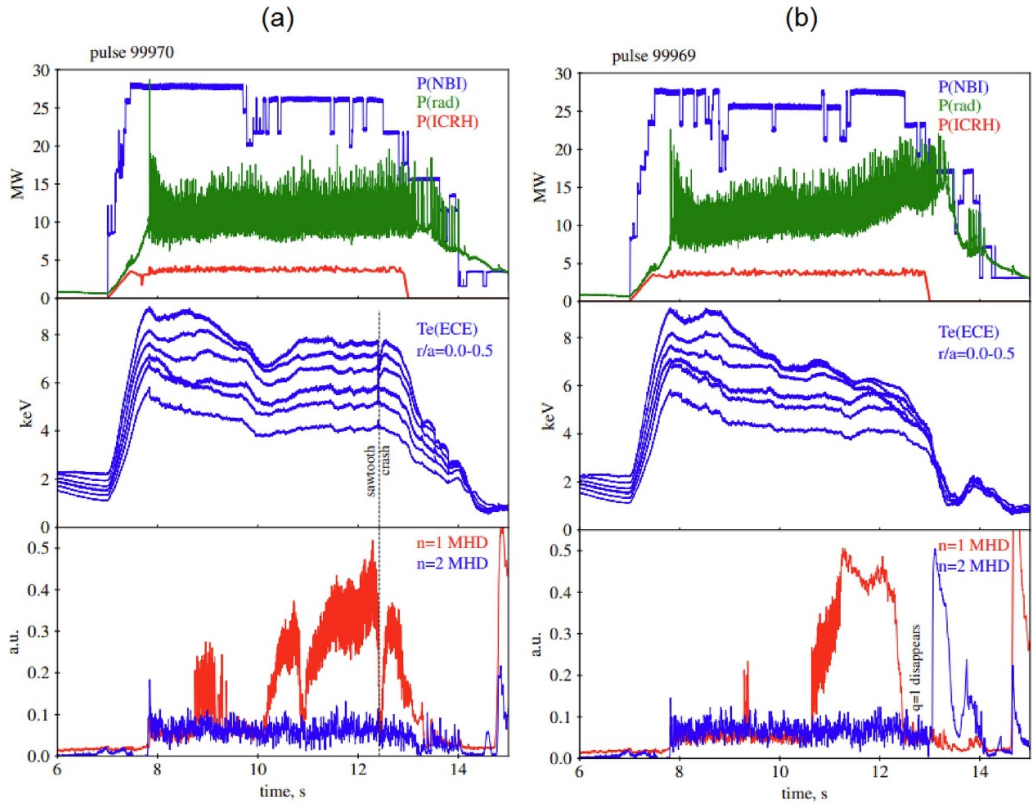

Figure 10. Examples of pulse evolution throughout the heating phase. From top to bottom: NBI, ICRH and radiated power, electron temperature (ECE) at different radii, MHD activity through Mirnov coils signal correlation for toroidal mode numbers $n = 1$ and $n = 2$. (*a*) #99970 stationary pulse with fishbones transitioning to $n = 1$ and sawtoothing plasma. (*b*) #99969 core impurity accumulation causes the hollowing of T_e profile, broadening of plasma current and emerging of $n = 2$ MHD activity.

fraction; the D/T ratio was reduced to ∼10/90 D/T, slowly increasing towards 15/85 by the end of the discharge flattop phase. The measured D/T ratio is roughly consistent with the balance of D and T particles introduced into the discharge by means of D-NBI and T-gas injection. It is important to note that the isotopic ratio measurements performed in the subdivertor are slow, so the time evolution shown in figure 9 does not necessarily reflect the time evolution of the isotope ratio in the plasma in the early phase of the heating flattop.

All pulses were hybrid scenario H-mode discharges adapted to the high toroidal magnetic field value of 3.86 T, as described in section 3. The safety factor (q) profile was pretailored via a fast plasma current ramp up to the 'overshoot' 3.1 MA value and subsequently ramped down to the target 2.5 MA [1]. In this way, a broad low shear profile with $q(0) > 1$ was achieved at the beginning of the H-mode phase. In the absence of a flexible current drive mechanism in these plasmas, the q-profile inevitably evolved throughout the 5 s flattop duration. The exact evolution of the q-profile is closely related to the electron temperature profile (or plasma resistivity), which in turn varied depending on the impurity content of the plasma and the balance of core radiation versus applied heating.

The q-profile evolution could be inferred through the changing pattern of the core magnetohydrodynamic (MHD) instabilities. In the initial phase of all discharges (0–2 s), no significant MHD activity could be seen. Typically, around 2.5 s after start of the heating phase, the first fishbone activity appears, indicating that $q(0)$ is close to unity. Subsequently, depending on the impurity penetration and electron temperature profile evolution, fishbones may transition into a continuous $n = 1$ MHD mode activity and eventually to sawtoothing plasma, indicating that $q(0)$ has decreased below unity (see figure 10(*a*)). Conversely, in the cases with high-Z core impurity accumulation and hollowing of the electron temperature profile, the plasma current profile broadened and $q(0)$ increased instead. This evolution was accompanied by disappearance of fishbones and emergence of higher n MHD instabilities later in the discharge (see figure 10(*b*)) [27].

Core impurity accumulation was the main factor limiting the stability of the pulses, which was partially mitigated by increasing the gas fuelling rate at the cost of fusion performance. Three pulses in this experiment (listed in table 1) have not developed core electron temperature hollowness at the end of the 5 s flattop and could be considered steady, in the sense that high fusion performance could have been sustained for longer than 5 s if JET technical capability had allowed this. In these pulses, the electron temperature profiles remained peaked, the core radiation remained steady and there were no signs of deleterious MHD modes or reduction in fusion performance other than related to the loss of heating power. One of the stable pulses (#99960), the first in the series, had

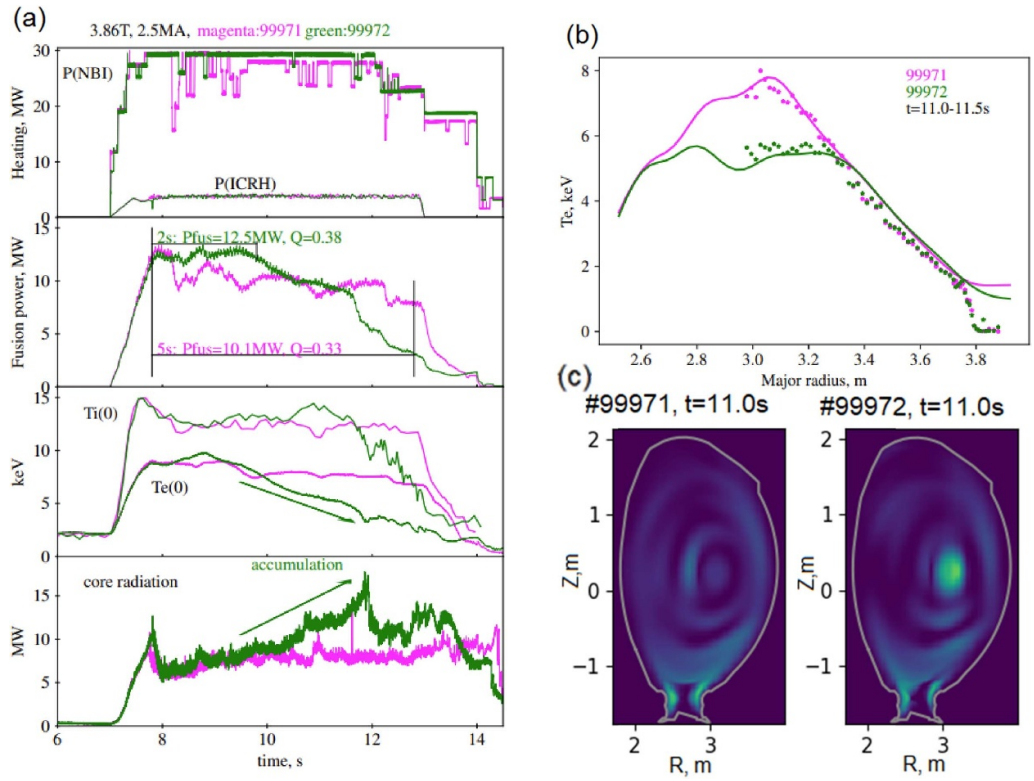

Figure 11. (*a*): Overview of the best performing pulses: #99971 (red) 5 s long stable fusion performance with non-steady NBI heating and highest $P_{\mathrm{fus}} = 10$ MW averaged over 5 s; and #99972 (blue) steady high NBI heating power achieving $P_{\mathrm{fus}} = 12.5$ MW over 2 s, later degraded by impurity accumulation. (*b*): T_{e} profiles at $t = 11$ s measured with Thomson scattering and ECE, indicating the cooling of the core, (*c*) tomographic reconstruction of plasma radiation measured with bolometry at $t = 11$ s for #99971 and #99972, showing the emergence of core localized radiation in #99972 during the period of degrading fusion power.

higher gas fuelling rate and hence a lower performance. In the following pulses, the gas fuelling was reduced in order to improve the fusion performance, but core impurity accumulation became the limiting factor. Eventually, a balanced recipe was found where a satisfactory plasma performance and discharge stability could be achieved simultaneously in pulses #99970 and #99971. Pulse #99964 was stable until the last second of the main heating phase, where high-Z impurity accumulation began due to a large drop in the NBI heating power. Pulses #99964, #99970 and #99971 had the same gas dosing waveform but the average NBI power was somewhat below the maximum due to various issues within the individual 15 NBI injectors. In the last pulse of the series, #99972, the full capability of the available D-NBI heating was achieved, but core impurity accumulation re-appeared and the discharge could not sustain stable performance for the full 5 s duration. In figure 11(*a*), the comparison between the two highest performance pulses is shown, #99971 and #99972.

The results of figure 11 suggest that a small difference in the average NBI heating power between #99971 and #99972 was sufficient to trigger the core high-Z impurity accumulation. The exact mechanism could not be identified yet. Clearly, an inward pinch of heavy impurities, presumably driven by a strong density peaking (see figure 12(*f*)), is present in these pulses as the increase in radiation and consequent plasma cooling is very localised at the magnetic axis (figures 10(*b*) and (*c*)). A delicate balance between the inward pinch and turbulent transport [28] is likely preserved in the steady pulse #99971 but could not be sustained in #99972. Note that the fusion power trace in #99971 follows closely the NBI power waveform (confirming the strong beam-target contribution to the neutrons) while the central ion and electron temperatures are comparable to #99972 in the beginning of the H-mode flattop but remain roughly constant throughout the discharge.

The higher heating power in #99972 could potentially contribute to a stronger tungsten sputtering from the divertor target and consequently larger influx of high-Z impurities. However, no appreciable difference in the plasma bulk radiation could be seen between these discharges until 9.5 s after the core plasma cooling started in #99972. Typically, in type I ELMy H-mode plasmas in JET-ILW, plasmas with lower ELM frequency are more susceptible to high-Z impurity accumulation as the ELMs provide a mechanism of flushing out the impurities from the plasma edge [11]. In these conditions, increase of the gas fuelling would usually cause an increase of the ELM frequency and hence a better resilience to high-Z impurity influx. However, in these T-rich H-modes, the ELM frequency $f_{\mathrm{ELM}} \sim 80$–100 Hz was already much higher than the typical value of 40–50 Hz in steady high-performance type I ELMy H-mode discharges. Furthermore, within the range of gas dosing rates used for this experiment and for injected D-NBI power of $\sim$29 MW, no appreciable response on the ELM frequency could be seen. No difference in ELMs characteristics is apparent between the pulses #99971 and #99972.

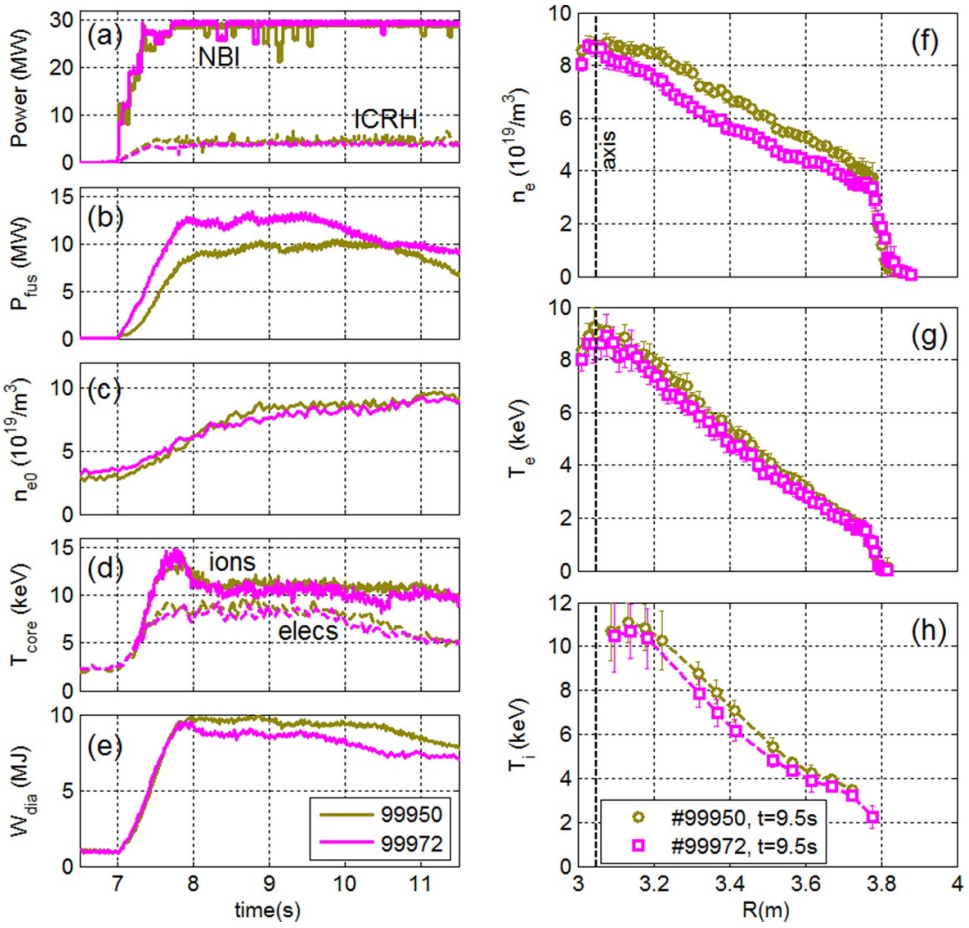

Figure 12. Comparison between 50/50 D/T (#99950 gold) and T-rich (#99972 magenta) hybrid discharges; (*a*) NBI + ICRH heating power; (*b*) fusion power, (*c*) central plasma density, (*d*) central electron (HRTS) and ion (CXRS) temperatures; (*e*) diamagnetic stored energy; (*f*) electron density profiles, (*g*) electron temperature profiles, (*h*) ion temperature profiles.

The stored energy of these tritium-rich hybrid H-modes is lower than for a typical type I ELMy H-mode in JET-ILW at similar plasma current and injected power. Figure 12 shows a comparison between a 3.4 T, 2.3 MA hybrid 50/50 D/T discharge #99950 and a 3.86 T, 2.5 MA T-rich discharge #99972. The pulses have similar heating power (*a*) but the tritium-rich discharge shows ∼3 MW of additional fusion power generated (*b*). The central ion and electron temperatures (*d*) are comparable in the first part of the discharge but the plasma stored energy (*e*) is lower in the T-rich scenario. The fishbone activity (not shown) appears at the same time in both discharges indicating that the core q-profiles are closely matched. The electron density and temperature profiles (*f*), (*g*) measured at $t = 9.5$ s with high-resolution Thomson Scattering (HRTS) [29] and the ion temperature profiles (*h*) by active charge exchange spectroscopy (CXRS) [30] are shown in the right column of figure 12. It can be seen that the difference in confinement comes largely from the pedestal and volume averaged plasma density, but the bulk electron and ion temperatures are also somewhat lower in the T-rich pulse. Note that the plasma density near the magnetic axis (figure 12(*c*)) is similar in these pulses, which implies larger density peaking in the T-rich pulse.

Figure 13(*a*) compares the electron density (from HRTS) and the ion temperature profiles (from edge CXRS) in the pedestal region for pulses #99950 (50–50 D-T type I ELMy hybrid H-mode) and #99972 (T-rich hybrid H-mode) at $t = 9.5$ s, illustrating in detail that the main differences between these pulses come from the pedestal densities. Figure 13(*b*) shows how the ELM behaviour is very different in these two discharges: pulse #99950 shows more typical Type I ELMs at a frequency of ∼40 Hz while in pulse #99972 the ELM's are smaller in amplitude and much more frequent (80–100 Hz). Pulse #99972 has larger effective isotope mass ($A_{\rm eff} \sim 2.85$) and plasma current. Consequently, the observed differences between these pulses is opposite to the conventional H98(y,2) H-mode scaling [31] and JET-ILW pedestal scaling for different $A_{\rm eff}$, which show the pedestal density to increase with effective mass [32]. These observations indicate that the pedestal of the T-rich H-mode discharges is not characteristic of a type I ELMy regime, and its pressure is likely limited by another type of edge MHD instability. This conclusion is supported by linear MHD stability analysis performed for both pulses as shown on figure 14 (for details of pedestal stability analysis see e.g. [33]). The colour code on the figure represents the growth rate of the peeling-ballooning modes, and the black line is the calculated stability boundary. The experimental point on figure 14(*b*) for the discharge #99950 (type I ELMy) is found close to the stability boundary, within

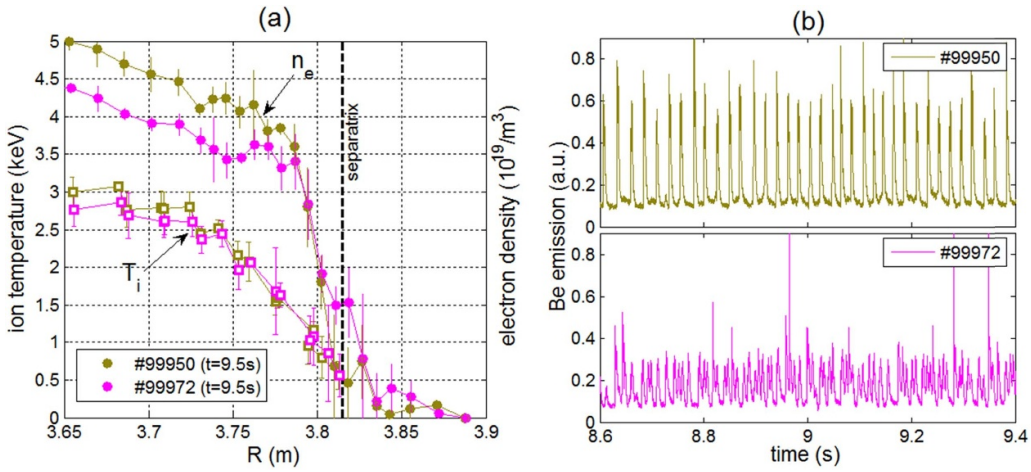

Figure 13. (*a*) Electron density (HRTS) and ion temperature (edge CXRS) profiles vs mid-plane plasma radius in the pedestal region for pulses #99950 (50–50 D-T type I ELMy hybrid H-mode) and #99972 (T-rich hybrid H-mode with small ELMs) at $t = 9.5$ s; The dashed line indicates the separatrix position according to EFIT; (*b*) Beryllium line intensity at the outer divertor (same scale) illustrating the different ELM dynamics in the two discharges.

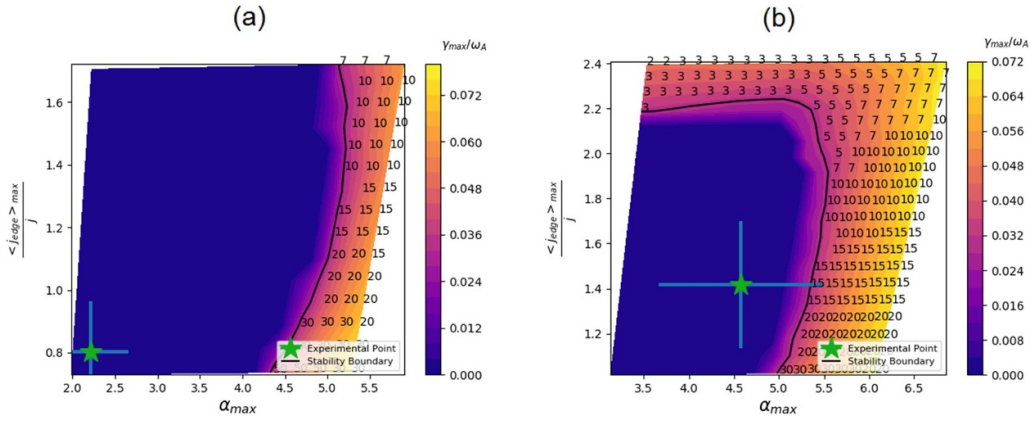

Figure 14. (*a*) Pedestal stability diagram of T-rich pulse #99972. (*b*) Pedestal stability diagram of 50/50 D/T pulse #99950 with type I ELMs.

the error bars, while the pedestal of the T-rich pulse #99972 (figure 14(*a*)) is found deep in the stable area.

It should be noted that the level of gas fuelling affects the pedestal performance, and the gas fuelling of these two pulses cannot be compared directly since the 50/50 D/T hybrid discharges use mixed D/T gas fuelling and the choice of the gas injection location is also different. It was not possible to determine whether reducing the gas fuelling in the tritium-rich pulse would bring the pedestal performance close to the 50/50 D/T case, since reduction of the gas fuelling caused high-Z impurity accumulation. Therefore, despite yielding higher fusion power, the T-rich pulses could not reach the higher values of H-mode confinement time observed in some of the 50/50 D/T hybrid pulses. Figure 15 summarises the fusion performance versus plasma stored energy as measured by the diamagnetic loop ($W_{\rm dia}$) for the T-rich and 50/50 DT hybrid pulses. For the same value of the stored energy, the T-rich pulses produced ~50% larger fusion power which is consistent with the expectations from predictive modelling carried out in preparation of this scenario, as outlined in section 3.

However, the extrapolations from 50/50 D/T hybrid scenario in section 3.1 to the tritium-rich with D-NBI heating which were made using TRANSP simulations that did not take into account the fusion enhancement due to ICRF heating of the fuel D ions (reactions between ions in the RF tail and thermal ions). According to ETS simulations [21], this accounts for a non-negligible contribution to the fusion enhancement, as discussed later in section 6. To experimentally quantify the effect of fundamental D heating on the fusion productivity in this scenario, pulse #99965 was run with modulated ICRF power (see figure 16). The pulse experienced impurity accumulation (likely due to lack of constant ICRF heating power throughout the main heating phase) but the modulation of fusion power was clearly visible. $Q_{\rm RF} = \Delta P_{\rm fus}/\Delta P_{\rm RF} \sim 0.7$ is estimated from the $P_{\rm fus}$ modulation amplitude. The central ion temperature is also clearly modulated with ICRF ($\Delta T_{\rm i}/\Delta P_{\rm RF} = 0.5$ keV MW^{-1}) showing that this RF heating scheme produces strong ion heating in the plasma centre, as expected from theory (see section 6).

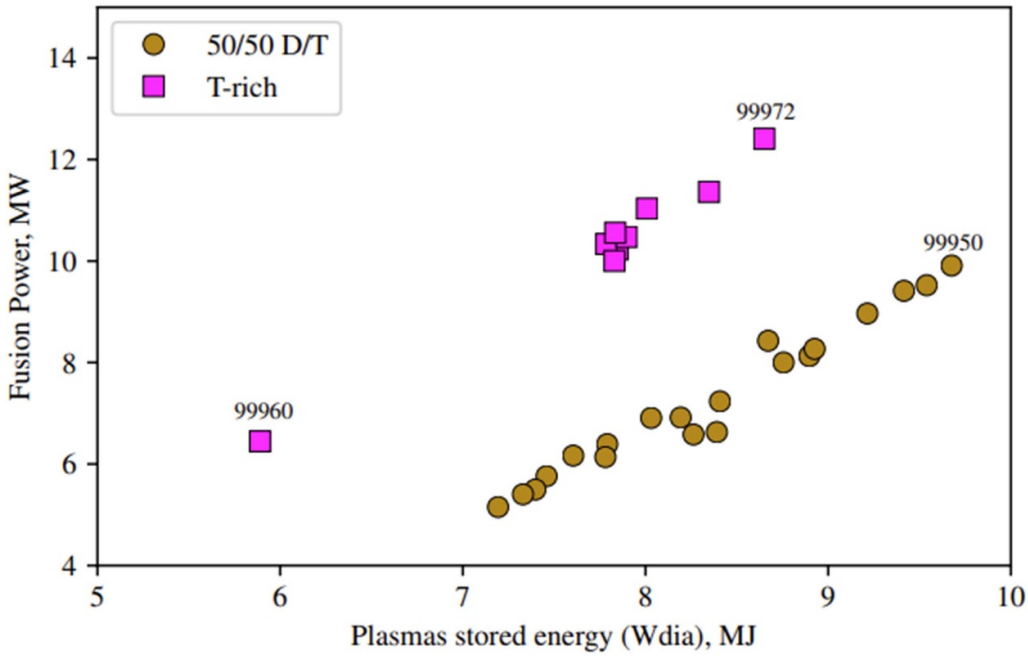

Figure 15. Generated fusion power versus plasma diamagnetic energy (W_{dia}) for the tritium rich pulses (magenta) and 50/50 D/T hybrid pulses (gold). The data for each pulse is averaged over the time window of $t = 8$–10 s.

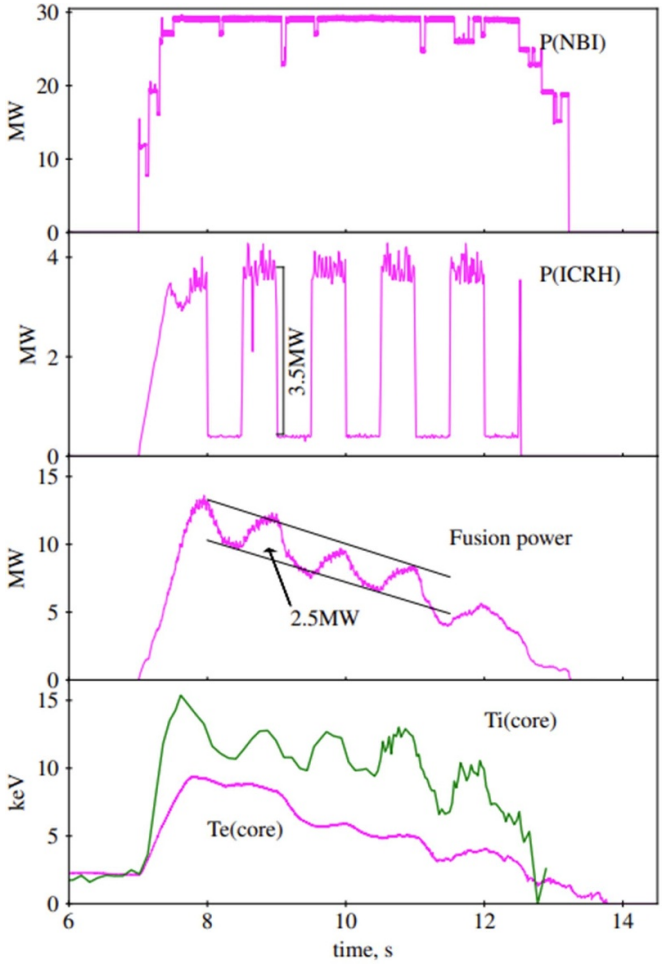

Figure 16. ICRF power modulation in tritium-rich pulse #99965 and the effect on the produced fusion power. From top to bottom: NBI power, ICRH power, fusion power output, core T_{e} (ECE) and T_{i} (x-ray spectrometer) values—notable T_{i} modulation.

6. Interpretative TRANSP and ETS analysis of the high fusion power discharges

The highest steady fusion performance discharge #99971 has been modelled with the TRANSP code [16]. Electron temperature and density profiles were measured by the HRTS diagnostic [29], ion temperature and plasma rotation by means of charge exchange recombination spectroscopy on Neon X impurity lines [30]. Small quantities of neon were injected into the discharges specifically to enable this measurement in the essentially carbon-free JET-ILW plasma. The D/T ratio was set as measured by the subdivertor Balmer-alpha spectroscopy in the plasma exhaust as shown in figure 9. The radial profile of the D/T ratio was approximately uniform in the simulation, with the standard adjustments made in the TRANSP code to accommodate the radial distribution of the fast ions and fusion products consistently with the imposed electron density profile. It should be noted that the plasma D/T composition could be different from the composition assumed in the TRANSP simulation, in particular in the initial phase of the discharge where the plasma density is increasing from the Ohmic to H-mode values in presence of strong D-NBI fuelling.

Figure 17 outlines the fusion performance of pulse #99971 as modelled by TRANSP (run L36) with these settings. The predicted fusion power is approximately 15% larger than the measured fusion power, with the overprediction reaching 25% during the first 1 s of the discharge. The thermonuclear fusion power fraction is estimated around ∼7% of the total fusion power towards the end of the flattop where the $n_{\mathrm{D}}/(n_{\mathrm{D}} + n_{\mathrm{T}})$ ratio reaches 12%.

According to these TRANSP simulations, acceleration of the D-NBI ions by ICRF heating contributes ∼7% to the total fusion power (the acceleration of the thermalized D ions is not accounted for). Calculation of the RF-induced acceleration of NBI ions within TRANSP is implemented via a Monte-Carlo 'kick' operator [34], which modifies slowing down NBI particles' energy each time they pass through the ICRF resonant layer. To quantify the effect of RF acceleration of D ions on the total fusion power, this operator has been switched off in otherwise identical TRANSP run L73 (see figure 17). However, the kick operator within the TRANSP code has only been validated for the hydrogen minority ICRH which contributes to the fusion power via acceleration of the fast D-NBI ions at the 2nd harmonic resonance. In case of the fundamental deuterium resonance scheme used in this experiment, both fast D-NBI ions and thermal deuterium ions are being accelerated, but the TRANSP code is presently unable to describe the acceleration of the thermal D ions and hence the total RF enhancement of the generated fusion power in this situation. This problem is discussed in details in [16] along with a proposed 'ad-hoc' scheme to overcome this limitation of TRANSP. As explained in [16], the total fusion power predicted by TRANSP in these T-rich discharges will increase by ∼10% if the acceleration of the bulk D ions is taken into account, which would bring the total neutron discrepancy to ∼25%.

NBI + ICRF heating/slowing-down simulations for the discharge #99971 were also performed using the ETS heating and current-drive workflow [21]. The kinetic profiles (input) and equilibrium were taken from the TRANSP run L36 shown above. The workflow computes the NBI and ICRF power deposition/absorption profiles and solves the Fokker-Planck equation for all the ion species present in the plasma, including self-collisions and NBI + ICRF synergy. The resulting distribution functions of the bulk and beam ions are then used to compute the D-T neutron profiles and the general fast ion properties. The NBI losses (first orbit losses and shine-through) amount to approximately 2.5 MW of the $P_{\mathrm{NBI}} = 29$ MW applied and were not considered in the simulations.

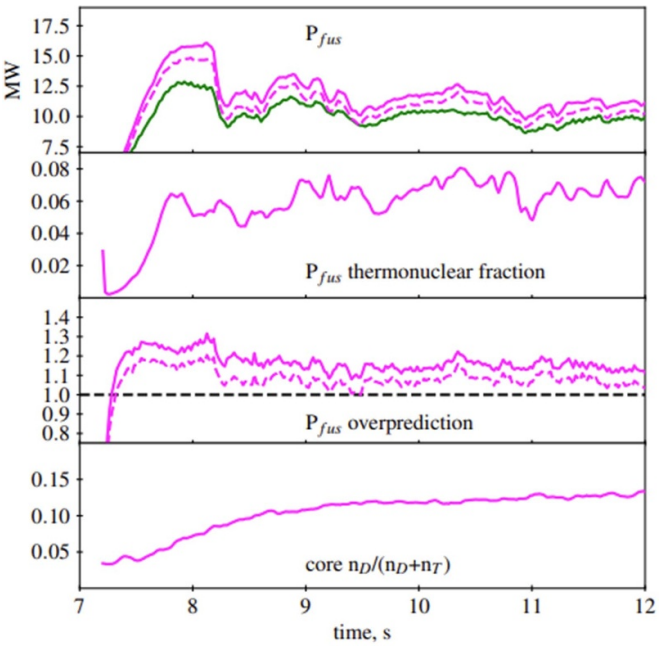

Figure 17. Output of fusion performance in the interpretative TRANSP run 99971 L36. From top to bottom: predicted (magenta) and measured (green) fusion power, fraction of thermonuclear reactions, ratio of predicted to measured fusion power (neutron deficit), core $n_{\mathrm{D}}/(n_{\mathrm{D}} + n_{\mathrm{T}})$ ratio as in the TRANSP model. Dashed line indicates TRANSP simulation L73 without ICRF kick operator.

The results of the ETS simulations are summarized in figure 18: (*a*) NBI source deposition and ICRF power absorption profiles per species; (*b*) Fusion power profile obtained with the ICRF accelerated bulk and beam ion distribution functions. The dashed lines represent the fusion power profiles obtained with NBI only heating ($P_{\mathrm{ICRF}} = 0$) but otherwise identical parameters.

Figure 18 shows that the ICRF absorption is mostly localized near the magnetic axis, reaching power densities comparable to those of the NBI deposition despite the five times lower total power injected. The central ICRF absorption is dominated by the bulk D ions, but the D-beam ions absorb a considerable amount of the power since they have a broader absorption profile due to their large Doppler shift. Beryllium absorbs about 12% of the power at ∼0.3 m off-axis on the high-field side of the plasma.

The simulations were done with and without the effect of ICRF heating on the deuterium energy distribution function (denoted as 'NBI-only' and 'NBI + ICRH' on figure 18(*b*)), both using the same kinetic profiles. The fusion power

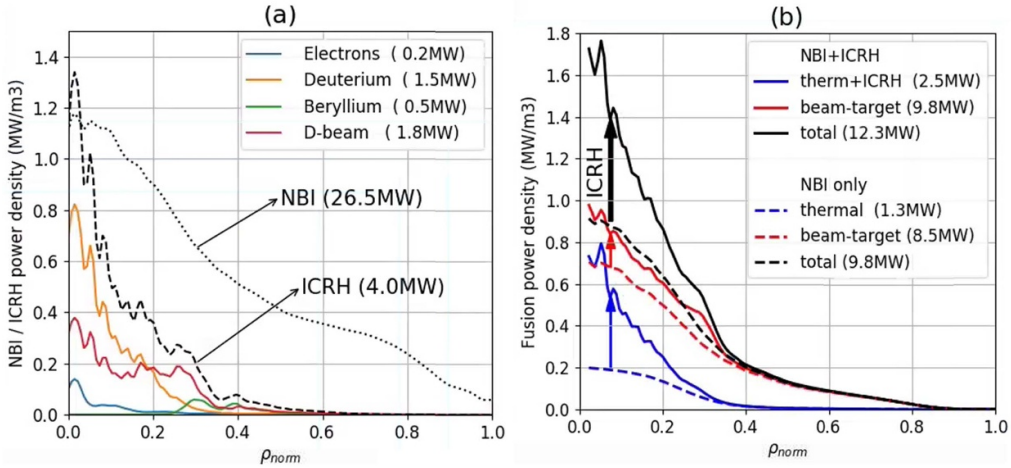

Figure 18. (*a*) NBI deposition (26.5 MW) and ICRH power absorption profiles per species (4 MW) computed with the ETS heating and current-drive workflow using the experimental parameters of the high-performance T-rich discharge #99971 at $t = 9$ s; (*b*) Calculated fusion power profiles accounting for the heated distribution functions of all the plasma species with NBI + ICRH heating. The dashed curves represent the values obtained with NBI only heating.

enhancement due to the ICRF is almost equally split between the acceleration of D-beam and D-bulk ions, giving an RF fusion enhancement of ∼20% (total $P_{\rm fus}$ increases from 9.8 MW to 12.3 MW, $Q_{\rm RF} = 0.6$). This number is slightly lower than the experimental observation made with modulation of the ICRF power (figure 16), but in the modelling the kinetic profiles were fixed thus the effect of the ion heating and change in $T_{\rm i}(0)$ was not accounted for.

For the interpretative simulations the assumption was made that the results of the H/D isotope experiments still apply for the T-rich plasmas and the D/T ratio in the plasma core is approximately equal to that of the plasma edge. Validation of that assumption by comparison of the predicted and measured neutron rate, as it was done for the H/D case, is not possible. Change in the core D/T isotope composition will strongly affect the balance between thermonuclear and beam-target fusion power components (see figure 3), but the total fusion power is less sensitive. The neutron overprediction which apparently affects the beam-target fusion will complicate such an analysis even further.

The ratio between thermonuclear and beam-target fusion in the T-rich plasmas can be inferred from the 14 MeV neutron spectra which are measured by a variety of diagnostics available at JET [35]. In particular, a synthetic diagnostic of the 14 MeV neutron spectra measured by the vertical diamond spectrometer using the distribution functions obtained in the ETS simulations for $n_{\rm D}/n_{\rm e} = 15\%$ showed that the ICRH + NBI fast particle modelling is in very good agreement with the experimental data as shown on figure 19 (solid line). For the purpose of a sensitivity study, the synthetic spectrum was also generated with varying D/T ratios. It was found that increasing the core $n_{\rm D}$ will worsen the agreement with the measured neutron spectra, as the consequent increase of the thermonuclear fraction with increase the peaking of the synthetic spectrum. This measurement of the fusion neutrons spectrum validates the assumption that the concentration of thermalized D in the plasma core remains low, in line with the expectations based on the H/D experiments and the integrated modelling results.

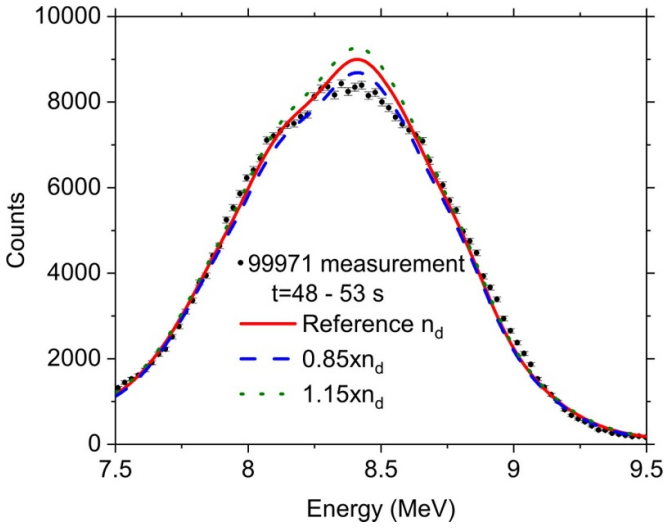

Figure 19. Neutron spectrum (shifted by 5.702 MeV from the 12C(n,α)9Be reaction [34]) measured by the vertical line of sight diamond detector versus reconstructed spectra for different D/T plasma compositions. Reference $n_{\rm D}/n_{\rm e} = 15\%$.

7. Quasi-linear modelling with JETTO-QuaLiKiz

Extensive integrated modelling was performed to validate the core transport models against the mixed H/D isotope experiments and to attempt a predict-first approach for the subsequent T-rich D/T discharges. This is extremely challenging due to the large sensitivity of the results to the pedestal parameters which are not known in advance and presently cannot be reliably predicted. Models such as [36, 37] can be used to predict pedestal pressure height at JET-ILW, but they are lacking the description of the mechanisms behind the formation

Table 2. Toroidal magnetic field, plasma current, input power and n_D/n_e concentration for three different normalized toroidal flux coordinates ρ_s in the plasma and for various simulations. Note that the extrapolations are more pessimistic than the validation for the boundary value of n_D/n_e, but the variation of n_D/n_e from the boundaries to the axis is similar for all the simulation.

Simulation	B_t (T)	I_p (MA)	Power (NBI + ICRF) (MW)	$n_D/n_e\rho_s = 0.85$	$n_D/n_e\rho_s = 0.2$	$n_D/n_e\rho_s = 0.0$
H-D Validation #94927 (figure 2(*b*))	2.8	2.4	25 + 0	0.12	0.21	0.24
D-T Extrapolation (figure 20)	3.85	2.7	31 + 8	0.25	0.3	0.33
D-T Validation #99971 (figure 20)	3.86	2.5	30 + 3.5	0.10	0.14	0.17

of the density pedestal. Some progress has been made in that domain recently (see e.g. [38]), but at the time when the predictive modelling for DTE2 campaign has been made, this information was not yet available. And it should be noted that the existing models are only applicable to type I ELMy H-modes, while the observed T-rich plasmas is unlikely to fall into the same category as it was shown on figure 14. However, despite the uncertainties in the plasma boundary, the ratio n_D/n_e was found to be remarkably flat from the pedestal to the magnetic axis in all the simulations. This provided confidence, prior to the experiment, in the absence of deuterium accumulation for high power, D-T discharges.

All the modelling described below was performed within the JINTRAC [39] framework, using JETTO as the 1.5D core transport solver. NCLASS [40] was used as the neoclassical transport model and QuaLiKiz [41, 42] as the core turbulent transport model. PENCIL [43], PION [44] and FRANTIC [45] were used for the NBI, ICRF and neutral particle source respectively. The impurities were modelled with SANCO [46] and the magnetic equilibrium was evolved self-consistently using ESCO [47].

Firstly, a set of low plasma current and low power (1.4 MA/1.7 T, $P_{\text{D-NBI}} = 8$ MW) mixed H/D isotopes experiments were successfully reproduced in integrated modelling, including ratios of isotope density profiles observed to be flat independently of the particle sources [5, 48]. The subsequent higher power H/D experiments were then modelled (described in section 2) and once again the integrated modelling was able to reproduce the experiment [49]. These results have proven the ability of the implemented modelling tools to describe the behaviour of the ion components in JET-ILW plasmas with high NBI heating power and strengthen the confidence in the subsequent extrapolations to D-T scenarios.

For predictive runs of the T-rich experiment, previous simulations of pure D pulse #92398 and extrapolations to D-T [28] were used as a template. Input power, toroidal magnetic field, plasma current and isotope content were adjusted to match the values that were expected in the T-rich experiment (table 2). Kinetic profiles (T_e, T_i, n_e) evolved fully self-consistently in the simulations, and the boundary conditions at $\rho = 0.8$ were set based on the empirical scaling for H-mode pedestal as described in [28]. The simulations projected a fusion gain of 5 MW (+30%) over otherwise identical simulations for 50/50 D/T scenario with balanced D-NBI and T-NBI heating. Nearly flat (table 2) concentration of deuterium was again obtained in the modelling, but the levels of deuterium predicted for the high performance D-T discharges were slightly overestimated with respect to the actual measurements obtained subsequently during the experiments. The predicted profiles are shown by the purple lines in figure 20.

Finally, the model was used interpretatively to simulate the high fusion power T-rich pulse #99971. For the boundary conditions (set at $\rho = 0.85$), the electron density and the ion and electron temperature profiles were taken from the interpretative TRANSP run L36, averaged over the 8.5–9.0 s time interval. The q-profile was taken from the deuterium hybrid pulse #97781 which was well diagnosed and produced successful modelling in previous work [49]. For the deuterium concentration at the boundary, a value of $n_D/n_e = 0.1$ was imposed, in line with the subdivertor gas composition measurements of pulse #99971 (figure 9). The results of this validation are shown by the black lines in figure 20.

Since QuaLiKiz is an electrostatic code, often an ad-hoc electro-magnetic stabilization factor is applied to better reproduce the experiment when electromagnetic effects are expected to be important. In these cases, the ion temperature gradient passed to QuaLiKiz is multiplied by the $W_{\text{thermal}}/W_{\text{total}}$ ratio, which effectively increases the ITG threshold. This stabilization mechanism has been studied for NBI fast ions [50], but in this modelling W_{total} also includes fast particles from other sources. In this particular discharge, the alpha pressure is not negligible. While turbulence stabilization by fast ions in MeV energy range has been observed to occur in specific conditions [51, 52], it is not clear whether the alpha pressure plays a role in this experiment. The ad hoc electromagnetic stabilization may therefore be too stabilizing in this case and cause an overestimation of the core plasma pressure. Both cases, with and without the ad-hoc correction, were run for comparison (figure 20, green and black curves respectively).

Fair agreement with the experiment was reached on the electron and ion temperature profiles. The central T_i is underpredicted in the case without the electro-magnetic effects and overpredicted in the opposite, suggesting that electromagnetic effects are present but weaker than what is calculated by the proxy (as expected from the considerations given above).

The density peaking was overestimated in both cases. Nevertheless, the crucial result of the isotope profiles remaining relatively flat over the whole plasma radius is maintained, with a change in concentration of ∼7%–12% from the boundaries to the axis depending on the assumption for the electromagnetic stabilization. Future work will include uncertainty quantification and comparison with predictions from TGLF [53], which includes electromagnetic effects. An interesting direction for future development, both for QuaLiKiz and TGLF, might be on consistently including the stabilizing

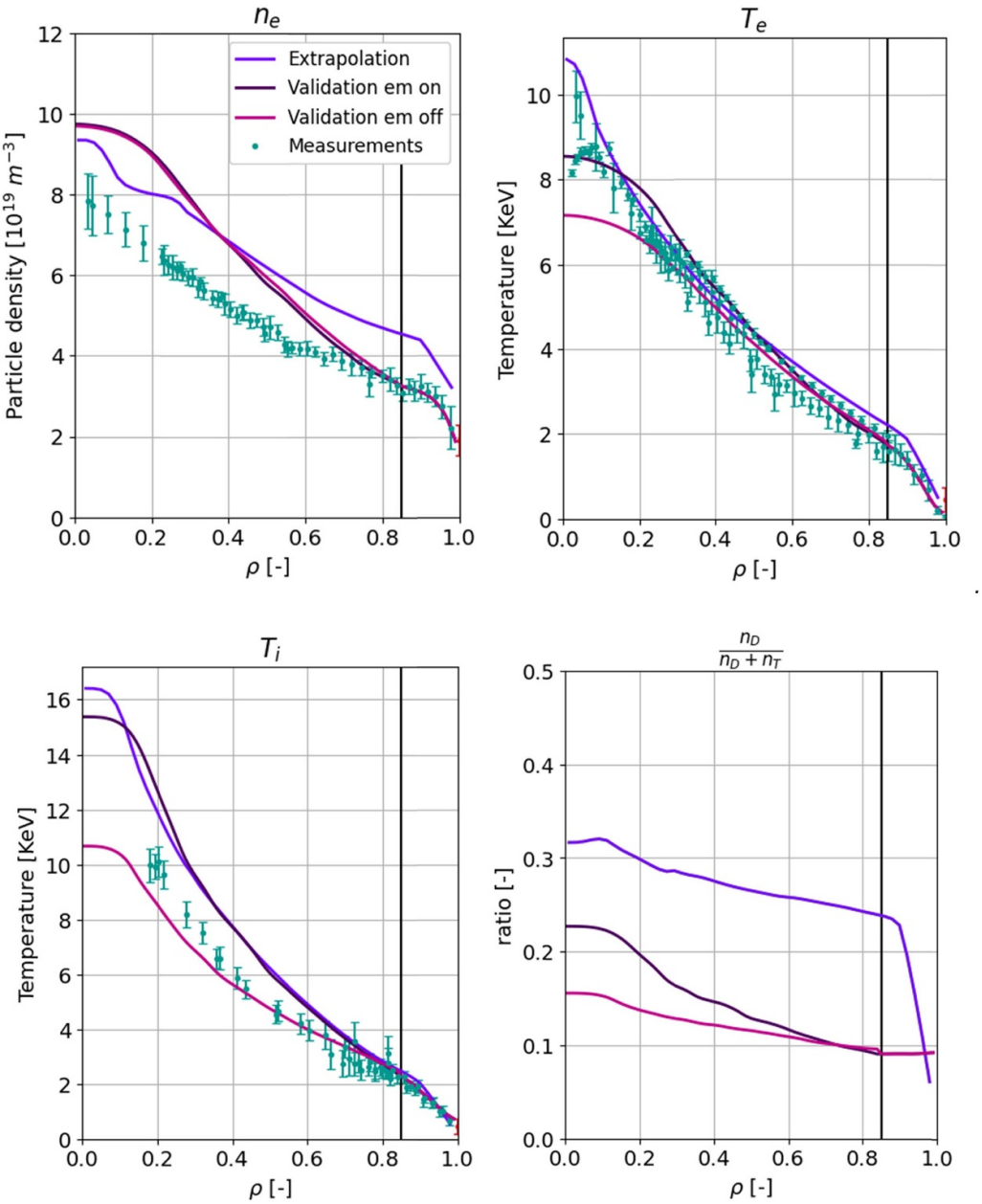

Figure 20. Kinetic profiles as measured, extrapolated and predicted imposing the experimental boundaries and heating as for the T-rich pulse #99971. The extrapolation performed before the experiment is shown in purple. The simulations performed after the experiment with and without the ad-hoc proxy for the electromagnetic stabilization effects are shown in pink and black respectively. The experimental data are shown in light green. The boundary condition is set at $\rho_{\text{tor}} = 0.85$, as marked by the vertical black line.

effect of fast ions, including alpha particles, as currently such effect is not well reproduced by quasi-linear models [52, 54].

8. Discussion and conclusions

A series of high fusion power discharges were produced at JET with Be/W wall during the DTE2 campaign in 2021. These H-mode pulses were designed to maximize the number of the beam-target fusion reactions between energetic deuterium minority ions injected into the plasma by means of NBI heating and thermal tritium ions which constituted the majority species of the plasma. This scenario was also characterized by fundamental deuterium resonance ICRF heating which boosted the fusion performance further by ∼20%. In line with the theoretical predictions, consistently high values of generated fusion energy were achieved in a series of pulses. Pulse #99971 generated the world record high value of $E_{\text{fus}} = 59$ MJ, of which 50.5 MJ were generated within a 5 s time window giving the average $P_{\text{fus}} = 10.1$ MW.

A tritium-rich hybrid H-mode plasma was developed with D/T ratio of ∼15/85, which was determined by the ratio between the number of deuterium atoms injected by means of the NBI heating and the number of tritium atoms injected as a

gas. The D/T ratio was approximately constant in the whole plasma volume as been found previously in mixed isotope plasmas and can be explained using first-principle based transport models [5, 6]. The core D/T ratio was validated by means of neutron spectroscopy and was corroborated by modelling of the neutron production in terms of the sensitivity to the plasma composition.

While some pulses in the series were steady and potentially could have lasted longer than the programmed 5 s long high fusion power phase, in many of cases the duration of the high-performance phase was limited by core accumulation of high-Z impurities. The impurity accumulation could be mitigated by increasing the gas dosing at some cost in fusion performance, but the exact mechanism of triggering or avoiding the accumulation is not yet fully understood and is the subject of on-going studies which will be reported in separate publications. It should be noted although that high density peaking (which presumably caused a strong neoclassical impurity pinch) was observed in these discharges. Since the generation of high fusion power in these plasmas relies on maximising the source of NBI particles in the plasma core, high density peaking is intrinsic to this scenario and could potentially be the limiting factor for sustained fusion performance in this JET-ILW plasmas.

Based on the studies of the effect of isotope mass on the type I ELMy H-mode pedestal, as reported in this NF special issue [32, 55], it was expected that the tritium-rich scenario would have a higher density pedestal with large low frequency ELMs compared to the D/T counterpart. Somewhat surprisingly, the experimental observation was rather opposite—the pedestal pressure was lower than the one observed in the 50/50 D/T hybrid scenario and the ELMs were of smaller amplitude and higher frequency. Due to experimental time limitations at the end of DTE2, when these experiments were executed, it was not possible to study in detail the confinement properties of these plasmas and this could be a subject of study for a next DT campaign.

Interpretative modelling of the high-performance T-rich discharge #99971 was performed with TRANSP, ETS and JETTO-QuaLiKiz. TRANSP is a widely used code, benchmarked on a large number of plasmas and has been used to interpret the fusion performance of all the scenarios performed during DTE2 [16, 56], but it does not include the ICRF acceleration of the D or T fuel ions. The ETS suite of codes used for this work, on the other hand, is better adapted for interpretation of the fusion performance of the T-rich scenario due to a more comprehensive description of the impact of ICRF heating on the deuterium energy distribution functions. Good agreement between the measured and the predicted fusion power using the ETS workflow was found, and the impact of ICRF heating compared reasonably well with the results of an ICRF power modulation experiment in pulse #99965. On the other hand, TRANSP results have shown a significant overprediction of the neutron rate despite of the neglection of the ICRF effects on the thermal D. The cause of the disagreement could not yet be identified and is the subject of on-going analyses [57]. JETTO-QuaLiKiz proved to be able to correctly predict the isotope composition. The uncertainty of the predicted density and temperature profiles proved however to be large, particularly with respect to the implementation of the electromagnetic effects. Even with a good prediction of the profiles, the fusion power was overestimated, similarly to what was observed in TRANSP. Improved treatment of electromagnetic effects and fast ions stabilization are interesting directions for future work and development.

While it was demonstrated that the hybrid T-rich scenario with ∼100 keV D-NBI injection is capable to produce ∼50% more fusion power than the 50/50 D/T hybrid plasma counterpart, it must be emphasized that this scenario cannot be exploited in an energy producing fusion power plant where the plasma heating must be self-sustaining and dominated by alpha particle heating that arises from the thermonuclear fusion reaction. Nonetheless, realization of a smaller size fusion device as a source of neutrons has been discussed in the past (e.g. [58]). The JET-ILW T-rich scenario demonstrated in this work is perfectly suitable for this purpose and could provide large 14 MeV neutron fluxes from driven burn in smaller-scale devices. This would require neutral beam ions with moderate injection energy (100–200 keV), which is much less demanding from the engineering point of view than the high energy NBI systems generally required by thermonuclear reactors.

The fundamental ICRF heating of D ions described here, on the other hand, does not rely on the presence of D beam ions and could be used either in T-rich plasmas (with a fraction of Deuterium) to directly enhance fusion reactivity in RF only machines or in 50/50 D/T plasmas to produce core ion heating in thermonuclear reactors. It is applicability for ITER is currently under study [59].

The JET machine is well suited for implementation of this scenario from several perspectives. NBI heating delivered fast D ions at energies corresponding to the highest D-T reaction cross-section (100–120 keV). At the same time, the plasma density is optimal for deposition of a significant fraction of the NBI power in the hot plasma core while ensuring a tolerable NBI shine-through. The right combination of available high toroidal magnetic field and low frequency ICRF heating power allowed using fundamental deuterium resonance heating to accelerate a fraction of the thermalized D ions to optimal energies. At the same time, the JET aspect ratio is sufficiently large to accommodate the core fundamental deuterium resonance and to avoid the 2nd harmonic tritium resonance at the low field side. In JET with carbon wall, the highest performance H-mode plasmas were generally achieved without additional gas dosing and relied solely on the fuelling by NBI. Achieving tritium-rich plasma using a high level of T edge gas fuelling with pure D-NBI would not be possible in a C-wall machine owing to T retention, so having the ITER-like metal Be/W wall was probably essential for the success of this experiment. At the same time, despite the demonstration of the record fusion energies, the maximum capacity of this scenario on JET-ILW has not yet been reached. The ICRF power was limited to 4 MW due to the unavailability of the ILA (ITER-like antenna) and was likely not sufficient to mitigate the core impurity accumulation. The scenario performance thus had to be compromised in order to achieve stationary conditions. The

NBI heating system only had ∼53% of power delivered at the main energy ∼110 kV. The rest of the power was injected as half and 1/3 energy fractions which have a much smaller contribution to the total fusion power. Additionally, the lower energy beam fractions delivered a considerable part of the total injected deuterium particles and therefore contribute to increased plasma dilution. Optimization of the balance between available ICRF and NBI power and use of NBI injectors with larger full energy fraction, together with bringing the plasma performance in line with the best 50/50 D/T hybrid pulses could significantly improve the efficiency of this scenario.

Acknowledgments

This work has been carried out within the framework of the EUROfusion Consortium, funded by the European Union via the Euratom Research and Training Programme (Grant Agreement No. 101052200—EUROfusion) and from the EPSRC [Grant No. EP/W006839/1]. To obtain further information on the data and models underlying this paper please contact PublicationsManager@ukaea.uk. The Swiss contribution to this work has been funded by the Swiss State Secretariat for Education, Research and Innovation (SERI). Views and opinions expressed are however those of the author(s) only and do not necessarily reflect those of the European Union, the European Commission or SERI. Neither the European Union nor the European Commission nor SERI can be held responsible for them.

ORCID iDs

M. Maslov https://orcid.org/0000-0001-8392-4644
E. Lerche https://orcid.org/0000-0003-4584-3581
F. Auriemma https://orcid.org/0000-0002-1043-1563
E. Belli https://orcid.org/0000-0001-7947-2841
C. Bourdelle https://orcid.org/0000-0002-4096-8978
A. Chomiczewska https://orcid.org/0000-0003-4931-728X
A. Dal Molin https://orcid.org/0000-0003-0471-1718
J. Eriksson https://orcid.org/0000-0002-0892-3358
J. Garcia https://orcid.org/0000-0003-0900-5564
J. Hobirk https://orcid.org/0000-0001-6605-0068
I. Ivanova-Stanik https://orcid.org/0000-0002-2766-8612
A. Kappatou https://orcid.org/0000-0003-3341-1909
D.L. Keeling https://orcid.org/0000-0002-3581-7788
V. Kiptily https://orcid.org/0000-0002-6191-7280
D. Kos https://orcid.org/0000-0002-9550-4329
R. Lorenzini https://orcid.org/0000-0001-8353-4857
E. De La Luna https://orcid.org/0000-0002-5420-0126
C.F. Maggi https://orcid.org/0000-0001-7208-2613
P. Mantica https://orcid.org/0000-0001-5939-5244
M. Nocente https://orcid.org/0000-0003-0170-5275
G. Pucella https://orcid.org/0000-0002-9923-2770
D. Rigamonti https://orcid.org/0000-0003-0183-0965
M. Salewski https://orcid.org/0000-0002-3699-679X
E.R. Solano https://orcid.org/0000-0002-4815-3407
Ž. Štancar https://orcid.org/0000-0002-9608-280X
G. Stankunas https://orcid.org/0000-0002-4996-4834
H. Sun https://orcid.org/0000-0003-0880-0013
D. Van Eester https://orcid.org/0000-0002-4284-3992

References

[1] Hobirk J. *et al* 2023 *Nucl. Fusion* **63** 112001
[2] Garzotti L. *et al* 2023 Development of high current baseline scenario for high deuterium-tritium fusion performance at JET *Nucl. Fusion* submitted
[3] IAEA ENDF database (available at: www-nds.iaea.org/exfor/e4explorer.htm)
[4] Maslov M. *et al* 2019 High fusion power in tritium rich scenario in JET, O5.104 *46th EPS Conf. on Plasma Physics* (*Milan, 8–12 July 2019*) (available at: http://ocs.ciemat.es/EPS2019PAP/pdf/O5.104.pdf)
[5] Maslov M. *et al* 2018 *Nucl. Fusion* **58** 076022
[6] Bourdelle C., Camenen Y., Citrin J., Marin M., Casson F.J., Koechl F. and Maslov M. 2018 *Nucl. Fusion* **58** 076028
[7] Jacquet P. *et al* 2022 ICRH Operations and Experiments during the JET-ILW tritium and DTE2 campaign *AIP Conf. Proc. 24th Topical Conf. on Radio-frequency Power in Plasmas* (*Annapolis, Maryland, US, 26–29 September 2022*)
[8] Mantsinen M. *et al* 2023 *Nucl. Fusion* **63** 112015
[9] Lerche E., Van Eester D., Krasilnikov A., Ongena J. and Lamalle P. 2009 *Plasma Phys. Control. Fusion* **51** 044006
[10] Start D.F.H. *et al* 1999 *Nucl. Fusion* **39** 321
[11] Joffrin E. *et al* 2014 *Nucl. Fusion* **54** 013011
[12] Breslau J., Gorelenkova M., Poli F., Sachdev J., Pankin A., Perumpilly G., Yuan X. and Glant L. 2018 USDOE Office of Science *TRANSP Computer Software*
[13] Goldston R.J., McCune D.C., Towner H.H., Davis S.L., Hawryluk R.J. and Schmidt G.L. 1981 *J. Comput. Phys.* **43** 61–78
[14] Ongena J.P.H.E., Voitsekhovitch I., Evrard M. and McCune D. 2012 *Fusion Sci. Technol.* **61** 180–9
[15] Brezinsek S. *et al* 2013 *Nucl. Fusion* **53** 083023
[16] Štancar Ž. *et al* Overview of interpretive modelling of fusion performance in JET DTE2 discharges with TRANSP *Nucl. Fusion* submitted
[17] Garcia J., Challis C., Gallart D., Garzotti L., Görler T., King D. and Mantsinen M. 2017 *Plasma Phys. Control. Fusion* **59** 014023
[18] Kalupin D. *et al* 2013 *Nucl. Fusion* **53** 123007
[19] Strand P. *et al* 2018 Towards a predictive modelling capacity for DT plasmas *27th IAEA Fusion Energy Conf. (FEC 2018)* (*India, 22–27 October 2018*) TH/P6-25 (available at: https://nucleus.iaea.org/sites/fusionportal/Shared%20Documents/FEC%202018/fec2018-preprints/preprint0451.pdf)
[20] Van Eester D. *et al* 2022 *Plasma Phys. Control. Fusion* **64** 055014
[21] Lerche E. *et al* 2022 Fundamental ICRF heating of Deuterium ions in JET-DTE2 *AIP Conf. Proc. 24th Topical Conf. on Radio-frequency Power in Plasmas* (*Annapolis, Maryland, US, 26–29 September 2022*)
[22] Lerche E. and Van Eester D. 2008 *Plasma Phys. Control. Fusion* **50** 035003
[23] Lerche E. *et al* 2020 *AIP Conf. Proc.* **2254** 030007
[24] Horton L.D. *et al* 1999 *Nucl. Fusion* **39** 993
[25] Vartanian S. *et al* 2021 *Fusion Eng. Des.* **170** 112511
[26] Christopher Klepper C. *et al* 2022 *IEEE Trans. Plasma Sci.* **50** 4970–9
[27] Pucella G. *et al* 2021 *Nucl. Fusion* **61** 046020
[28] Casson F.J. *et al* 2020 *Nucl. Fusion* **60** 066029

[29] Frassinetti L., Beurskens M.N.A., Scannell R., Osborne T.H., Flanagan J., Kempenaars M., Maslov M., Pasqualotto R. and Walsh M. 2012 *Rev. Sci. Instrum.* **83** 013506
[30] Hawkes N.C., Delabie E., Menmuir S., Giroud C., Meigs A.G., Conway N.J., Biewer T.M. and Hillis D.L. 2018 *Rev. Sci. Instrum.* **89** 10D113
[31] ITER Physics Expert Group on Confinement and Transport 1999 *Nucl. Fusion* **39** 2175
[32] Schneider P.A. *et al* 2023 *Nucl. Fusion* **63** 112010
[33] Saarelma S., Alfier A., Beurskens M.N.A., Coelho R., Koslowski H.R., Liang Y. and Nunes I. 2009 *Plasma Phys. Control. Fusion* **51** 035001
[34] Kwon J.-M., McCune D. and Chang C.S. 2007 Enhancement of NUBEAM for the simulation of fast ion and RF-wave interaction based on the quasi-linear theory, Bulletin of the American Physical Society *49th Meeting of the Division of Plasma Physics (Orlando, FL)*
[35] Nocente M. *et al* 2022 *Rev. Sci. Instrum.* **93** 093520
[36] Snyder P.B., Groebner R.J., Hughes J.W., Osborne T.H., Beurskens M., Leonard A.W., Wilson H.R. and Xu X.Q. 2011 *Nucl. Fusion* **51** 103016
[37] Saarelma S., Challis C.D., Garzotti L., Frassinetti L., Maggi C.F., Romanelli M. and Stokes C. 2018 *Plasma Phys. Control. Fusion* **60** 014042
[38] Saarelma S., Connor J.W., Bilkova P., Bohm P., Field A.R., Frassinetti L., Fridstrom R. and Kirk A. 2023 *Nucl. Fusion* **63** 052002
[39] Romanelli M. *et al* 2014 *Plasma Fusion Res.* **9** 3403023
[40] Houlberg W.A., Shaing K.C., Hirshman S.P. and Zarnstorff M.C. 1997 *Phys. Plasmas* **4** 3230–42
[41] Bourdelle C., Citrin J., Baiocchi B., Casati A., Cottier P., Garbet X. and Imbeaux F. 2016 *Plasma Phys. Control. Fusion* **58** 014036
[42] Citrin J. *et al* 2017 *Plasma Phys. Control. Fusion* **59** 124005
[43] Challis C.D., Cordey J.G., Hamnén H., Stubberfield P.M., Christiansen J.P., Lazzaro E., Muir D.G., Stork D. and Thompson E. 1989 *Nucl. Fusion* **29** 563–70
[44] Eriksson L.G., Hellsten T. and Willen U. 1993 *Nucl. Fusion* **33** 1037–48
[45] Tamor S. 1981 *J. Comput. Phys.* **40** 104–19
[46] Alper B. *et al* 1994 Impurity transport of high performance discharges in JET *21st EPS Conf. on Controlled Fusion and Plasma Physics* (*Monpellier*, *27 June–1 July 1994*) (available at: https://inis.iaea.org/collection/NCLCollectionStore/_Public/28/032/28032669.pdf)
[47] Cenacchi G. and Taroni A. 1988 *JETTO: A Free-Boundary Plasma Transport Code* (available at: https://inis.iaea.org/collection/NCLCollectionStore/_Public/19/097/19097143.pdf)
[48] Marin M., Citrin J., Bourdelle C., Camenen Y., Casson F.J., Ho A., Koechl F. and Maslov M. 2020 *Nucl. Fusion* **60** 046007
[49] Marin M. *et al* 2021 Integrated modelling of multiple-ion tokamak discharges *PhD Thesis* (available at: https://pure.tue.nl/ws/portalfiles/portal/176607703/20210901_Marin_hf.pdf)
[50] Citrin J *et al* 2013 *Phys. Rev. Lett.* **111** 155001
[51] Mazzi S *et al* 2022 *Nat. Phys.* **18** 776–82
[52] Garcia J. JET Contributors 2022 *Plasma Phys. Control. Fusion* **64** 104002
[53] Staebler G.M., Kinsey J.E. and Waltz R.E. 2005 Gyro-Landau fluid equations for trapped and passing particles *Phys. Plasmas* **12** 1–24
[54] Citrin J. and Mantica P. 2023 *Plasma Phys. Control. Fusion* **65** 033001
[55] Frassinetti L. *et al* 2023 *Nucl. Fusion* **63** 112009
[56] Kim H.-T. *et al* 2023 *Nucl. Fusion* **63** 112004
[57] Weisen H. *et al* 2017 *Nucl. Fusion* **57** 076029
[58] Voss G., Davis S., Dnestrovskij A., Kirk A., Knight P.J., Loughlin M., O'Brien M.H., Sychugov D., Tabasso A. and Wilson H.R. 2008 *Fusion Eng. Des.* **83** 1648
[59] Schneider M., Lerche E., Van Eester D., Hoenen O., Jonsson T., Mitterauer V., Pinches S.D., Polevoi A.R., Poli E. and Reich M. 2021 *Nucl. Fusion* **61** 126058